Synthesis of Polymer-Stabilized Silver-Iron Oxide Nanocomposite for Antibacterial Application

Samrawit Roba Tasse

A Thesis Submitted to

The Department of Applied Chemistry

School of Applied Natural Science

Presented in Partial Fulfillment of the Requirement for the Degree of Masters of Science in Applied Chemistry (In Analytical Chemistry)

Office of Graduate Studies

Adama Science and Technology University

September, 2023

ASTU, Adama, Ethiopia

Synthesis of Polymer-Stabilized Silver-Iron oxide Nanocomposite for Antibacterial Application

Samrawit Roba Tasse

Advisor: Defaru Negera (PhD)

Co-Advisor: Buzuayehu Abebe (PhD)

A Thesis Submitted to

The Department of Applied Chemistry

School of Applied Natural Science

Presented in Partial Fulfillment of the Requirement for the Degree of Masters of Science in Applied Chemistry (In Analytical Chemistry)

Office of Graduate Studies

Adama Science and Technology University

September, 2023

ASTU, Adama, Ethiopia

DECLARATION

I hereby declare that this Master Thesis entitled “Synthesis of polymer-stabilized silver-iron oxide nanocomposite for Antibacterial Application” is my original work. That is, it has not been submitted for the award of any academic degree, diploma, or certificate in any other university. All sources of materials that are used for this thesis have been duly acknowledged through citation.

_____	_____	_____
Name of student	Signature	Date

RECOMMENDATION

We, the advisor(s) of this thesis, hereby certify that we have read the revised version of the thesis entitled "Synthesis of polymer-stabilized silver-iron oxide nanocomposite for Antibacterial Application" prepared under our guidance by Samrawit Roba submitted in partial fulfillment of the requirements for the degree of Mater's of Science in applied chemistry (Analytical chemistry stream). Therefore, we recommend the submission of a revised version of the thesis to the department following the applicable procedures.

_____	_____	_____
Major Advisor/Supervisor	Signature	Date
_____	_____	_____
Co-advisor/Co-supervisor	Signature	Date

APPROVAL PAGE

We, the advisors of this thesis entitled “Synthesis of polymer-stabilized silver-iron oxide nanocomposite for Antibacterial Application” and prepared by Samrawit Roba; hereby certify that the recommendation and suggestions made by the board of examiners are appropriately incorporated into the final version of the thesis.

Major Advisor	Signature	Date
Co-advisor	Signature	Date

We, the undersigned, members of the Board of Examiners of this thesis by Samrawit Roba have read and evaluated the thesis entitled “Synthesis of polymer-stabilized silver-iron oxide nanocomposite for Antibacterial Application” and examined the candidate during open defense. This is, therefore, to certify that the thesis is accepted for partial fulfillment of the requirement of the degree of Master of Science in Analytical Chemistry.

Chairperson	Signature	Date
Internal Examiner	Signature	Date
ዶ/ር ጥበቡ አለሙ አያኔ Dr. Tibebu Alemu Ayaan	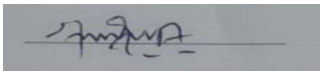	10/07/2023
External Examiner	Signature	Date

Final approval and acceptance of this thesis is contingent upon submission of its final copy to the Office of Postgraduate Studies (OPGS) through the Department Graduate Council (DGC) and School Graduate Committee (SGC).

Department Head	Signature	Date
School Dean	Signature	Date
Office of Postgraduate Studies, Dean	Signature	Date

ACKNOWLEDGEMENT

My profound gratitude goes to Almighty God, for the strength, wisdom, provisions, and guidance for the success of this thesis work. To Him alone, I ascribe all the glory.

I sincerely acknowledge my hard-working advisor: Dr. Defaru Negera for his constructive support, expert advice, technical assistance, and patience throughout my study period. I appreciate his tremendous encouragement, understanding, and arranging of research facilities. Sir, I appreciate the time you devoted to this work; and your experience. It is a great privilege and honor for me to be advised by him. Moreover, my heartfelt appreciation goes to my Co-Advisor Dr. Buzuayehu Abebe for his constructive feedback and suggestions that have been extremely valuable.

I would also like to thank the Department of Applied Biology for allowing me to use scanning electron microscopy and conduct Antibacterial Activity Applications, the Department of Materials Science Engineering for allowing me to use XRD instruments, Bahir Dar University for running TGA, FTIR, SEM-EDX and UV-DRS Spectra analysis.

Last but most importantly, I would like to extend my most profound gratitude to all my family members for their sincere love, help, and encouragement during the entire study period.

Finally, I would like to express my sincere gratitude to; Adama Science and Technology University for budget support, providing the necessary knowledge, assistance, and facilities to conduct my research work in their lab.

TABLE OF CONTENTS

Contents **page**

DECLARATION i

RECOMMENDATION ii

APPROVAL PAGE iii

ACKNOWLEDGEMENT iv

TABLE OF CONTENTS v

LIST OF TABLES ix

LIST OF FIGURES x

LIST OF ABBREVIATIONS xii

ABSTRACT xiii

1. INTRODUCTION 1

1.1 Background of the Study 1

1.2 Statement of Problem 4

1.3 Objectives 5

1.3.1 General objective 5

1.3.2 Specific objectives 5

1.4 Significance of the Study 6

1.5 Scope of the Study 6

2. LITRATURE REVIEW 7

2.1 Nanoscience and Nanotechnology 7

2.1.1 Nanoparticles 7

2.1.1.1 Semiconductor nanomaterials 8

2.1.1.2 Iron oxide nanomaterials 8

2.1.1.3 Silver nanoparticles 9

2.2 Nanocomposite 9

2.2.1 Ag-Fe_2O_3 nanocomposite 10

2.3 Polymers and Types of Polymers 10
2.3.1 Polyvinyl alcohol 11
2.3.2 Chitosan 11
2.4 Synthesis Methods of Nanoparticles 11
2.4.1 Physical methods 12
2.4.2 Chemical methods 13
2.4.2.1 Sol-gel methods 13
2.4.2.2 Solution combustion synthesis methods 14
2.4.2.3 Chemical reduction 15
2.4.3 Biological methods 15
2.5 Characterization Techniques of Nanoparticles 16
2.5.1 X-ray diffraction (XRD) 16
2.5.2 Fourier transform infrared (FTIR) spectroscopy 16
2.5.3 Scanning electron microscopy (SEM) 17
2.5.4 UV-Visible Spectroscopy (UV-vis) 17
2.5.5 Photo luminescence (PL) 17
2.5.6 Thermogravimetric analysis (TGA) 18
2.6 Application of Nanomaterials 18
2.6.1 Application of silver nanoparticles 19
2.6.2 Application of Fe_2O_3 nanoparticles 20
2.6.3 Application of Ag-Fe_2O_3 nanocomposite 21
2.7 Antibacterial Application of Ag-Fe_2O_3 Nanocomposite 22
3. MATERIAL AND METHODS 23
3.1. Chemicals and Instruments 23
3.1.1. Chemicals and reagents 23
3.1.2. Apparatus 23
3.2 Experimental procedure 23

3.2.1 Synthesis of silver and iron oxide (Fe_2O_3) nanoparticles 23
3.2.2 Synthesis of Ag-Fe_2O_3 nanocomposites (SICs) 24
3.3 Characterization 25
3.3.1. Thermo Gravimetric analysis (TGA) 25
3.3.2.X-ray diffraction (XRD) 26
3.3.3. UV–Vis diffused reflectance (UV–Vis DRS) spectroscopy 26
3.3.4. Fourier transform infrared (FT-IR) spectroscopy 26
3.3.5. Morphological and composition characterization 26
3.4. Antibacterial Test 27
3.4.1. Disk diffusion methods 27
3.5. Data Analysis 28
4. RESULT AND DESSCUSION 29
4.1 Synthesis of Ag-Fe_2O_3 Nanocomposite 29
4.2. Characterization 30
4.2.1. Thermogravimetric (TGA) analysis 30
4.2.2. X - ray diffraction (XRD) result analysis 31
4.2.3. UV-visible diffuse reflectance (UV-Vis - DRS) spectra and Bandgap Analysis 34
4.2.4. Fourier transforms infrared (FT-IR) results analysis 36
4.2.5. Photoluminescence result analysis 37
4.2.6. SEM-EDX analysis 38
4.3. Antibacterial Activity Analysis 40
4.3.1. Antibacterial susceptibility test 40
4.4 Mechanism of Antibacterial Activity 43
5. CONCLUSION AND RECOMMENDATION 45
5.1 CONCLUSION 45
5.2. RECOMMENDATIONS 45
6. REFERENCE 46

LIST OF TABLES

Table 1.Amount of different percentage of precursor 24
Table 2.Crystallite size of Fe_2O_3 and Ag-Fe_2O_3 33
Table 3.Calculations of average particle sizes of and Synthesized NCs Samples.....34
Table 4.FTIR vibration frequency of Fe_2O_3 NPs and 15SIC before and after calcination. 37
Table 5. Antibacterial activity of SICs sol-gel synthesized Fe_2O_3 NPs and 0.5SIC and 15SIC. 42

LIST OF FIGURES

Figure 1. Schematic illustration of the production of nanoparticles via several processes. 12
Figure 2. Applications of various metallic nanoparticles 19
Figure 3. Flowchart for the synthesis of Fe_2O_3 nanoparticles and SICs by sol-gel combustion method.....25
Figure 4.The color change of silver and silver-iron oxide nanocomposite in the synthesis process. A) SIC and B) silver NP. 30
Figure 5. The TG-DTA thermal stability analysis: the TG-DTA plots of PAV-Fe_2O_3 NPs, respectively. At about 390 ^{o}C, pure Fe_2O_3 NPs were obtained.....30
Figure 6. XRD pattern of PVA, Ag, Fe_2O_3 NPs, and SICs nanocomposites: (a) XRD patterns of Fe_2O_3 and different percentages of SIC, (b and c) Magnified view XRD pattern for Fe_2O_3 and SICs; there is no higher or lower angle shift on the XRD pattern of the composites than single Fe_2O_3, confirming the non-inclusion of silver in the Fe_2O_3 lattice. The inset in Fig. 6c is the structure models of Ag and Fe_2O_3 NPs. crystals developed by the software 3D Visualization for Electronic Structural Analysis (3D-VESTA) from the crystallographic information file (CIF) data. 32
Figure 7. The UV-vis-DRS spectra of SICs materials: (a) The UV-vis-DRS spectra of SICs, (b) are the direct and indirect Kubelka-Munk (K-M) plots. 35
Figure 8. The FTIR spectroscopic chemical bonding analysis: the FTIR spectra of Fe_2O_3 NPs and 15SIC before and after calcination. 36
Figure 9.The photoluminescence (PL) spectra of Fe_2O_3 NPs and 15SIC materials: (a) The PL spectra of Fe_2O_3 and (b) PL spectra of 15SIC. A slight intensity reduction for the composites was observed compared to Fe_2O_3, indicating the presence of some electron-hole recombination hindrance due to doping. 37
Figure 10.FESEM morphological and EDS elemental mapping analysis for 15SIC: (a) and (b) are the FESEM images for SICs at 1 μm and 500 nm magnifications, respectively. The porosity occurred was due to gas evolution. (c) The EDS layered image; (d) the FESEM image, from which the EDS mapping analysis was conducted. The green, red, and aqua images are the elemental mapping results for silver, oxygen, and iron, respectively. The good dopant elemental distribution on the Fe_2O_3 surface proves the potential of the sol-gel/solution combustion approach for synthesizing nicely distributed doped composites. 38
Figure 11. The EDX compositional analysis spectra for SICs show the presence iron, silver, and oxygen without any other impurities. The inset table in the EDX spectra shows the

composition of the elements in the proportion for silver and iron, also in accordance with the precursor's amount taken during synthesis. 39
Figure 12.Disk diffusion antibacterial activity evaluation of the sol-gel/combustion synthesized Fe_2O_3(a), 0.5SIC(b) and 155SIC(c) against P. aeruginosa, S. pyogenes, E. coli, and S. aureus. 43

LIST OF ABBREVIATIONS

Ag NPs	Silver nanoparticles
ATCC.	American Type Culture Collection
DMSO	Dimethyl sulfoxide
EDX	Energy Dispersive X-ray Spectrometry
FTIR	Fourier Transform Infrared
FWHM	Full-width half maximum
JPCDS	The Joint Committee on Powder Diffraction Standards
MNP	Magnetic nanoparticles
MRI	Magnetic Resonance imaging
NC	Nanocomposite
NNI	National Nanotechnology Initiative
NP	Nanoparticles
PNP	Polymer nanoparticles
PVA	Polyvinyl alcohol
ROS	Reactive oxygen species
SEM-EDX	Scanning electron microscope-energy dispersive x-ray spectroscopy
SIC	Silver iron oxide nanocomposite
UV-vis DRS	diffuse reflectance ultraviolet-visible spectroscopy
XRD	X-ray diffraction

ABSTRACT

Sol-gel-combustion synthesized nanoparticles (NPs) having reduced chemical toxicity have been focused globally and become an essential component of nanotechnology recently. In this study, silver-iron oxide nanocomposite (SICs) was synthesized by sol-gel combustion from PVA via a chemical, economic, and eco-friendly strategy. The presence of SICs were visually indicated by the color changes from light orange to light gray color. The sol-gel combustion synthesized SICs were characterized using thermogravimetric analysis (TGA), diffuse reflectance ultraviolet-visible spectroscopy (UV-vis/DRS), Fourier transform infrared (FTIR), X-ray diffraction (XRD), photo luminesce (PL) and scanning electron microscope/energy-dispersive X-ray (SEM–EDX) instruments. SIC FTIR result revealed functional groups that were analogous to PVA, which reduced and stabilized the nanocomposite. X-ray diffraction was signifying the crystal structure and the average crystallite size of SIC powder around 34.55 - 41.63 nm. The independent peak for both Ag and Fe_2O_3 crystals on the XRD pattern analysis without peak shift confirms the dominance of Schottky junction formation. Pure iron oxide obtained at 390 ℃. In Photoluminescence result the slight blue shift for the composites over Fe_2O_3 is probably due to the Ag-independent peak. Antibacterial efficacy of the sol-gel combustion synthesized (uncalcined) SIC against bacterial pathogens was assessed. In addition, 15SIC exhibited broad spectrum activities against Staphylococcus aureus, Streptococcus Pyogenes, Escherichia coli, and Pseudomonas aeruginosa with inhibition zones at 100 mg/mL of 18.3 ± 0.6, 22 ± 0.5, 21.6 ± 0.8 and 22.6 ± 0.3 mm, respectively. Pseudomonas aeruginosa (22.6) have shown maximum zone of inhibition and while least activity was seen against S. aureus. The 15SIC showed promising antibacterial action against human bacterial pathogens, making them useful in the medical field. The synthesized NC have great activity on gram negative bacteria than gram positive bacteria.

Keywords: *Silver- Iron oxide Nanocomposite, polyvinyl alcohol, Sol-gel-combustion method, Antibacterial activity, Disk diffusion method,*

1. INTRODUCTION

1.1 Background of the Study

According to the World Health Organization (WHO), The problem of AMR has gotten worse over the past few decades due to an increase in the frequency of MDR pathogen isolates from both hospital- and community-acquired illnesses. MDR bacteria is one of the most pressing issues facing the globe today since it can harm humans at every stage of life as well as the veterinary, agricultural, and health care sectors. vitro susceptibility testing is used to identify bacteria that are multidrug-resistant (MDR) when they are resistant to at least one antimicrobial agent from three or more antimicrobial classes. The use of antibiotics over time results in the natural evolution of antimicrobial resistance (AMR). On the other hand, AMR has evolved throughout the years due to the overuse and abuse of antibiotics(Alemayehu, 2021).

The majority of bacteria can be classified into two types: Gram-positive and Gram-negative. The main difference between such bacteria is their cell structures: Gram-positive bacteria have a thick layer of peptidoglycan in the cell walls, while the peptidoglycan layer of Gram-negative bacteria is thinner, and covered with another lipid membrane. In addition to a thin peptidoglycan layer, which is also present on the Gram-positive bacteria, Gram-negative bacteria have an outer membrane lipopolysaccharide. This layer acts as a barrier that prevents from entering negatively charged ROS(Russell, 2003). On the contrary, the cell membrane of Gram-positive has a less negative charge that allows penetration of negatively charged ROS (Gordon *et al*., 2011).Mostly, *Staphylococcus aureus and Streptococcus Pyogenes* are used to represent Gram-positive bacteria, and *Pseudomonas aeuruginosa and Escherichia coli*, Gram-negative bacteria, in antibacterial experiments(Fan *et al*., 2021).

As the antibiotic resistance of microbes to drugs grows, nanotechnology provides us an opportunity to resolve this problem. Metal NPs, referred to as nanobiotics, have been proposed as novel antibacterial agents. They have the potential to reduce or eliminate the continuous emergence of bacterial resistance. As nanotechnology has developed, Ag and iron oxide NPs have become widely used in antibacterial applications, especially in combatting antibiotic-resistant bacteria and nosocomial infections(Rautela *et al*., 2019). The interesting and unexpected properties of nanoparticles are attributed to their large surface area, and this dominates the contributions made by the small bulk of the materials (Rane *et al*., 2018).

Metal oxide NMs are one of the preferences as antibacterial active materials. Among several narrow-band semiconductors, novel characteristics properties of iron oxide such as abundance in the earth crust (6 wt%), low cost, environment-friendly, high surface area, and thermodynamically-stable have received greater significance. Besides, iron oxide has good surface area and utilizes about 20% of the solar spectrum (Jiamprasertboon *et al*., 2019; Sivula *et al*., 2011; Wang *et al*., 2019). This hematite iron oxide nanoparticle possesses a band gap of 2.1–2.2eV (Sangaiya & Jayaprakash, 2018). Depending on the applied temperature, among different crystalline polymorphs of Fe_2O_3, the α-Fe_2O_3 phase is more stable and easy to be formed (Lee & Xu, 2016). Iron oxide is vital in mediating the final heterogeneous chemical redox reaction of the target agent due to its high surface area and environmentally biocompatible properties (Cao & Wang, 2011). The novel antibacterial activity of Fe_2O_3 was also recently verified in different works (Haseena *et al*., 2020; Naz *et al*., 2019; Pallela *et al*., 2019). For example, Pallela et al. (Pallela *et al*., 2019) synthesized Fe_2O_3 with an average particle size of 16 nm. The antibacterial activity of Fe_2O_3 against *B. subtilis NCIM 2063, S. aureus NCIM 2079, E. coli 2065,* and *K. pneumonia NCIM 2327* bacteria was tested. Compared to the other, Fe_2O_3 shows enhanced antibacterial activity towards *B. subtilis.*

Metal oxide NPs has a large surface area and high surface energy property; consequently, they aggregate easily to one another. The aggregation of metal oxide NPs reduces the generation of the radioactive oxygen species due to the quenching of holes and electrons with neighboring aggregate electrons and holes, respectively (Jassby *et al*., 2012), which leading to diminishing the antibacterial activity. For this aggregation problem, nowadays, a polymer matrix has been effectively applied as a capping agent (Wu & Wu, 2015). Among numerous polymers, PVA is an eco-friendly, biocompatible, nontoxic, lubricant, biodegradable, water-soluble, and better film-forming agent (Hong *et al*., 2009; Madkour *et al*., 2019; Z. Zhang *et al*., 2017). It also has mechanical strength, which is used as a noble matrix for the formation of the NCs (Z. Zhang *et al*., 2016). Besides, its hydroxyl groups on the backbone carbon chain act as a source for the formation of hydrogen bonding and enhance the development of the NCs (Mallakpour & Adnany Sadaty, 2016). Therefore, optimizing the calcination temperature that assists the oxidation and removing volatile impurities such as the polymer matrix is also essential.

Effective doping of metal or metal ions, which creates either an n-type or p-type dopant, is one of the main significant ways to tune the electrical, magnetic, and optical properties. Besides, the incorporation of impurities also increases the surface-to-volume ratios, create crystal defect,

and traps charge carriers(Buonsanti *et al*., 2008; Jun *et al*., 2006; Rahman *et al*., 2019). The doping or forming a heterojunction of the Fe_2O_3 host with different bandgap materials such as silver improves the electron-hole recombination drawbacks of the host materials (K. Xu *et al*., 2017; M. Xu *et al*., 2020). Doping is either substitutional or interstitial insertion of the dopant in the host lattice, resulting in tuning the optical, electrical, and magnetic properties. The hard and soft (Lewis) acids and bases (HSAB) theory is crucial for regulating the host-dopant reactivity balance (Abebe & Murthy, 2022; Buonsanti & Milliron, 2013). The heterojunction is a band alignment between two or more semiconductors with different band gaps. Heterojunction between semiconductors boosts the surface area, charge transfer, and optoelectrical properties. The charge transfer process reduces electron-hole recombination, which is critical for several applications, such as antibacterial and catalysis (Yusuf *et al*., 2022). Eeffective inclusion and/or well-distribution of the dopants on the semiconductor's host surfaces can tune the properties of the host, increase the material's surface area, and improve the charge transfer process through the Schottky junction (Abebe & Murthy, 2022). Doping of silver (Ag) that has smaller ionic radius than Fe_2O_3 (host) believed resulting in quantifiable higher angle or a lower angle shift on the XRD pattern (Modwi *et al*., 2021)(Yıldırım *et al*., 2013). However, makes it difficult to substitute/interstitially dope Ag metal that has greater ionic radii in iron lattice with smaller ionic radii (Yin *et al*., 2017). Besides, silver is reduced easily by gaseous byproducts during combustion reactions (Nersisyan *et al*., 2017). Thus, the formation of a local contact or heterojunction dominates in place of interstitial or substitutional inclusion (Liu *et al*., 2019). The formation of Schottky contact between Ag and Fe_2O_3 results in the quenching of fluorescence light from Fe_2O_3, which improves the host-to-dopant charge transfer process, consequently extending the electron-hole lifetime (Ansari *et al*., 2013).

The synthesis of Ag and Fe_2O_3 NPs can be done using top-down or bottom-up methods (Alharbi, Alsubhi, and Felimban 2022). The synthesis of Ag and Fe_2O_3 NPs, like that of most nanomaterials, is mainly divided into three different processes: chemical, physical, and biological synthesis (Abdulsahib, 2021)**.** Metallic precursors, reducing agents, and stabilizing/capping agents are basically needed for chemical processes. The sol-gel method is a wet chemical approach that is widely utilized in nanomaterial development. This technique is used to create a variety of high-quality metal-oxide-based nanomaterials (Salem *et al*., 2022). Solution combustion is one of the wet chemical methods that involve an exothermic reaction of metal nitrates (oxidants) and an organic fuel. The fuel-oxidant ratio is one of the most

important parameters in determining the properties of the nanopowders synthesized using the combustion technique (Rane *et al*., 2018).

The antibacterial activity of the as-synthesized nanocomposite against *Pseudomonas aeuruginosa and Escherichia coli* (Gram-negative bacteria), *Staphylococcus aureus* and *Streptococcus Pyogenes* (Gram-positive bacteria) clinical isolate resistant strains were investigated. It was very small amount of Ag can effectively exhibit high antibacterial activity. The magnetic material enables the nanocomposite to be separated from the contaminated water (Demarchi *et al*., 2018).

The combination of magnetic properties of iron oxide nanoparticles and antibacterial properties of nanosilver predisposes these nanocomposites to use in disinfection and biomedical applications, where they can be used for targeted transport of an antibacterial agent and subsequent removal using an external magnetic field (Prucek *et al*., 2011). Considering all the above-indicated ideas of aggregation, surface area to volume ratio, and charge transfer property; this work aims to synthesize, poly (vinyl alcohol) (PVA) assisted silver doped iron oxide NCs using a simple sol-gel-solution combustion synthesis technique. This work also attempts to reduce the electron-hole recombination and enhance the charge transfer capability of the NCs by forming a heterojunction. The thermal stability, average crystallite size, and morphology of synthesized materials were confirmed by the TGA, XRD, UV-vis-DRS, FT-IR, PL and SEM-EDS analytical techniques. Using XRD analysis the approximate crystallite size of the materials was confirmed to be in the nanometer range. The EDS analysis was confirming the presence of predictable composition of the composites. The potential of the synthesized NPs and NCs towards antimicrobial activities were also studied.

1.2 Statement of Problem

Due to its intriguing qualities, such as a wide and direct bandgap, good thermal stability, a significant amount of exciting binding energy, and intense luminescence, silver and iron oxide nanocomposite have become a common asset and attracted interest from all over the world. In particular, conductivity, stability, efficacy, synergy, surface area, charge transfer, and activity features of the silver and iron oxide nanocomposite have produced antibacterial effects. The chemical production of polyvinyl alcohol-based silver and iron oxide nanocomposite and its use as an antibacterial agent are driven by a few fundamental issues. Microbial infectious

illnesses have developed into a severe health issue that has attracted global attention as a threat to human health that also includes economic and social repercussions. Infectious infections caused by bacteria are a serious issue in poor nations. It creates bacterial resistance to commonly used antibacterial, making it more challenging for communities to choose an effective antibacterial treatment. The rise of bacteria, viruses, and other pathogens that are resistant to medication has made it more challenging to control many infectious diseases today. At the same time, people with infections that are resistant to treatment may not be able to access or afford any of the current medications due to the high burden of infectious diseases. To partially cover this gap, silver and iron oxide nanocomposite synthesis for possible antibacterial agents is being studied. Various studies on the synthesis of silver and iron oxide nanocomposite (SIC) for antibacterial purposes have been conducted. This work uses PVA as a reducing and stabilizing agent to create silver and iron oxide nanocomposite via chemical means (sol-gel and solution combustion), and to test the antibacterial efficacy of the resulting material against various bacteria. The investigation is also focused on the first time to outline the potential use of stabilized polymer for nanocomposite as reducing, stabilizing, and capping agent in the synthesis of stabilized polymer silver-iron oxide nanocomposite and examine its antibacterial activities. The aims of this thesis are the synthesis and characterization of silver and iron oxide nanocomposite for antibacterial application.

1.3 Objectives

1.3.1 General objective

The general objective of this study was to Synthesis characterizes and study antibacterial application of SICs.

1.3.2 Specific objectives

- To synthesize Ag and Fe_2O_3 NPs and SICs using PVA as reducing agent (stabilizing agent).
- To characterize Ag NPs, Fe_2O_3 NPs and Ag-Fe_2O_3 NCs through common analytical techniques such as TGA, XRD, UV-DRS, FTIR, PL and SEM-EDX.
- To Evaluate performance of the synthesized materials against two gram-positive (*Staphylococcus aureus and Streptococcus Pyogenes*) and two gram-negative bacteria (*Pseudomonas aeuruginosa and Escherichia coli*) bacteria.

1.4 Significance of the Study

This study gives information for the scientific community about synthesis and antibacterial application of SICs. It also gave information on how to produce the NCs which are harmless and give basic knowledge about silver doped iron oxide nanocomposite. The outcome of this research can have a considerable effect on research and even on industrial activities as it serves as a basis for any scientific investigations of silver doped iron oxide nanocomposite. It can also bring a technology transfer and serve as background information for a researcher who wants to conduct further study on the topic under study and it provides information to prospects about various potential applications of polymer (polyvinyl alcohol) for synthesizing silver doped iron oxide nanocomposite using conventional synthesizing process. Additionally, using Ag-Fe_2O_3 nanocomposite for antibacterial purposes that are inexpensive and environmentally benign is beneficial. It will provide information on the actions of Ag nanoparticles and Fe_2O_3 and their composite nanoparticles in antibacterial application.

1.5 Scope of the Study

This research works was limited to synthesis, characterization of the synthesized nanocomposite using TGA, XRD, UV-DRS FTIR, PL and SEM-EDX technique. As well as study their application as antibacterial agent on gram positive bacteria (*Staphylococcus aureus and Streptococcus Pyogenes)* and gram-negative bacteria (*Escherichia coli and Pseudomonas aeuruginosa)* bacteria.

2. LITRATURE REVIEW

2.1 Nanoscience and Nanotechnology

Nanoscience is the study of matter's characteristics at the nanoscale, with a special emphasis on the distinct, size-dependent characteristics of solid-state materials(Mulvaney, 2015).The study of materials with dimensions between 1 and 100 nanometers (nm) is known as nanoscience. Nanotechnology is defined as "a science, engineering, and technology conducted at the nanoscale (1 to 100 nm), where unique phenomena enable novel applications in a wide range of fields, from chemistry, physics, and biology to medicine, engineering, and electronics" by the National Nanotechnology Initiative (NNI) in the United States. The ability to see, measure, manipulate, assemble, control, and manufacture matter at the nanoscale is known as nanotechnology. It is used to translate the theory of nanoscience into practical applications (Bayda *et al*., 2019). Nanotechnology is the capacity to control a single nanoscale object. It mostly entails the processing of separation, consolidation, and deformation of materials by one atom or one molecule. The basic and the key elements of nanotechnology are the ‘‘nanomaterials”(Kolahalam *et al*., 2019a).

2.1.1 Nanoparticles

Nanoparticles are of scientific interest as they are, in effect, a bridge between bulk materials and atomic or molecular structures. A bulk material has constant physical properties regardless of its size, but at the nanoscale, size- dependent properties are observed. The interesting and unexpected properties of nanoparticles are attributed to the large surface area, and this dominates the contributions made by the small bulk of the materials(Rane *et al*., 2018). Nanoparticle (NP) is a term used to describe particles with a dimension measured in nanometers. Nanoparticles, which come in a variety of shapes like spherical, triangular, cubic, pentagonal, rod-shaped, shells, elliptical, and more, are made up of a very small number of constituent atoms or molecules that have different properties from those found in their bulk counterparts. The random motion of the microscopic particles, quantum tunneling, discreteness of the energy, matter's uncertainty, dual nature of mass, and energy for wave particles are some other phenomena that nanoparticles displayed (Shehzad *et al*. 2018). Nanomaterials may be of different shapes like nanorods, nanoparticles, nanosheets which can be characterized based on their dimensionality. Nanomaterials with zero-dimensional are nanoparticles, one dimensional

is nanorods or nanotubes and two dimensional are generally films and layers type one(Kolahalam *et al*., 2019a).

2.1.1.1 Semiconductor nanomaterials

Semiconductor nanomaterials have metallic and non-metallic properties. They By altering it, it demonstrates different properties and exhibits large band gaps. These are commonly employed in electronic and photocatalytic devices(Kolahalam *et al*., 2019b).Semiconductor materials have properties halfway between metals and nonmetals, giving them a wide range of uses in the literature. Due to the huge bandgaps of semiconductor NPs, bandgap tuning resulted in significant changes in their properties. As a result, they're crucial in photocatalysis, photo optics, and electronic devices. Due to their optimal bandgap and band edge positions, several semiconductor NPs are particularly efficient in water splitting applications. These are usually organic-based NPs, and they're referred to as polymer nanoparticles (PNPs) in the literature. Typically, they are nano-spherical or nano capsular in form. The former are matrix particles with a solid overall mass, whereas the other molecules are adsorbed at the outside edge of the spherical surface. In the latter case, the solid mass is completely encapsulated within the particle(Salem *et al*., 2022).

2.1.1.2 Iron oxide nanomaterials

Among the different types of nanoparticles, hematite (iron oxide) is one of the most common, natural and environmental-friendly. It has a significant part in biogeochemical cycles of iron in the environment. There are different phases of iron oxide crystallites exhibited as hematite (α-Fe_2O_3), maghemite (γ-Fe_2O_3), goethite Fe (OH) and magnetite (Fe_3O_4). The hematite phase is considered as the more stable n-type semiconductor behavior. Nowadays, researchers have given more attention towards the stable hematite iron oxide for antibacterial application. The reason for choosing this α-Fe_2O_3 (hematite) iron oxide as a specific nanoparticle is only due to its low cost and being non-toxic, biocompatible and hence applied in biomedical field. This hematite iron oxide nanoparticle possesses a band gap of 2.1–2.2 eV(Sangaiya & Jayaprakash, 2018). Iron oxide is thermodynamically the most stable one due to its small size and large surface area (Annu *et al*., 2018).

Iron oxide nanoparticles were made into the core-shell bimetallic structures which enhance the efficiency due to their synergistic effect(George *et al*., 2018). Because they are superparamagnetic, iron oxide NPs are being investigated as a passive and active targeted imaging agent. They have an iron oxide core and a hydrophilic dextran or other biocompatible chemical coating to boost their stability (Haroon Anwar, 2018). Indeed, the biological properties of NPs are strongly associated with the physio-chemical nature of NPs as well as the capping molecules employed in salt precursor reduction and on the surface of NPs immobilize. The most probable explanation is the usage of biological products in the production of NPs, such as phenols, aldehydes, ketones, reducing acids, alkaloids, flavonoids, and, or, etc. The free radical scavenging efficacy has a direct relationship to antioxidant properties as well as behavior-like phenolic and flavonoid molecules(Al-Hakkani *et al*., 2021).

2.1.1.3 Silver nanoparticles

Because of their distinctive physical, chemical, and optical characteristics, silver nanoparticle is use in a wide range of applications. Numerous products that contain silver nanoparticles to stop bacterial growth on surfaces and in garments have been developed as a result of a resurgence in interest in the use of silver as a general antibacterial agent(Oldenburg, 2019). Due to the high coupling of the silver nanoparticles to particular wavelengths of incident light, the optical characteristics of silver nanoparticles are of interest. Over the past few years, silver nanoparticles (AgNPs) have become widely used in a variety of applications, including biomedicine, biosensors, catalysis, pharmaceuticals, antibacterial and photonics. AgNPs are typically small silver nanoparticles with unique electrical, optical, and magnetic properties that have a wide range of applications. Their size ranges from 1 to 100 nm (T. Galatage *et al*. 2021a). AgNPs have serious drawbacks like their low yield for penetrating bacterial biofilms and their concentration-dependent toxicity to human cells(Luengo *et al.*, 2020).

2.2 Nanocomposite

The nanocomposite is a polyphase solid material where one of the phases has one, two or three dimensions of less than 100 nm. Nanocomposites have a high surface to volume ratio which differs from typical composites(Kolahalam *et al*., 2019b). It is also defined as a technically tailored material comprising dissimilar constituents with disparate physical and chemical properties, which forms a discrete interface within the nanocomposite that it is composed of

two dissimilar material-matrix material and dispersed material, out of which at least one dimension of the dispersed material should be on nanoscale. Polymer nanocomposite is composed of a matrix material and a polymer as one of the constituents, along with a dispersed material like single or multiple nanoparticles within the parent polymer matrix. Decades ago, polymer nanocomposites emerged as an alternative to conventional structural materials due to their greatly-amended electrical properties, mechanical robustness, chemical resistance and steadiness, easy and adaptable processing technique, and low-cost effectiveness. Polymer nanocomposites have been proved to be a promising multifunctional material finding their scope of usage in packing industry, sporting goods and gears, air-water-land transportation sector and also in bio-medical engineering applications(Shukla & Saxena, 2021).

2.2.1 Ag-Fe_2O_3 nanocomposite

Nanomaterials which have magnetic behavior, such as Fe_2O_3 or Ag-Fe_2O_3, are good candidates for super-paramagnetism. Magnetic resonance imagining (MRI) investigations also utilize iron oxide nanoparticles. The combination of Ag and Fe_2O_3 achieves the properties of both metals. Due to these properties, researchers have been interested in making a hybrid composite of Ag-Fe_2O_3 offering better catalytic, bactericidal, and bio-imaging properties(Al-Zahrani *et al*., 2022).

2.3 Polymers and Types of Polymers

To overcome the problem of agglomeration, different kinds of stabilizing agents have been used during the AgNPs synthesis such as glucose, triethylenetetramine, poly(vinyl alcohol), chitosan, and 2-ami- noethanethiol(Nguyen *et al*., 2022). Metal nanoparticles must be produced with precise size and form, which requires capping agents such polymers, organic ligands, and surfactants. On the other hand, their complicated and debatable effects on the functionality of catalysts based on nanomaterials are difficult to quantify. It is true that a capping agent can act as both a "poison," decreasing active site accessibility, and a "promoter," resulting in higher yields and unanticipated selectivity control. The creation of the metal-ligand interphase, whose unique characteristics are in charge of the catalytic action, can be attributed to these occurrences. Therefore, understanding the structure of this interphase is essential for maximizing the creation of unique nanocatalyst designs. Long-chain hydrocarbons functionalized with heteroatoms are a common capping agent utilized in the manufacture of

nanoparticles. Biomolecules, The use of biomolecules to make homogeneous NPs has lately sparked interest due to their non-toxic nature and lack of arduous synthetic techniques. To produce NPs with a unique structure, amino acids serve as effective reducing and capping agents (Salem *et al*., 2022).

2.3.1 Polyvinyl alcohol

PVA is a semicrystalline synthetic polymer with overhanging hydroxyl groups. This polymer has been chosen for its very useful properties, biodegradability and biocompatibility, which make it a promising candidate for biomedical and food packing applications(Factori *et al*., 2021). Polyvinyl alcohol (PVA) has been widely utilized in biomedical applications such as drug delivery systems, contact lenses, artificial heart surgery, and wound dressings , cartilage replacements, surgical threads, owing to its specific properties such as non- toxicity, variety of molecular weights, high oxygen permeability, bio-degradability and good interactions with metal oxide nanoparticles(Hoque *et al*., 2018). PVA has a lot of medical applications and is used by virtue of elasticity and tensile strength in some polymers like chitosan. It can be used for coating of Ag, iron oxide, cellulose, titanium dioxide, and copper(I) sulfide nanoparticles(Ghaffari-Moghaddam & Eslahi, 2014).

2.3.2 Chitosan

Chitosan is composed of 2-amino-2-deoxy-β-d-glucan; a linear polysaccharide can be dissolved easily in water. Amino groups of Chitosan provide a hydrophilic environment compatible with the bio- molecules. Also, modification of pendants on chitosan provides significant advantages in biomedical applications, as for instance bio- sensors, hyperthermia treatment, tissue engineering, enzymatic assays, drug delivery, magnetic resonance imaging (MRI), cell separation, and clinical diagnostics because of their biodegradability and good biocompatibility. Among the various hydrophilic biopolymers, Chitosan has biocompatibility, excellent film- forming ability, high chemical modification responsivity, non-toxicity, high water permeability, cost-effectiveness etc (Hoque *et al*., 2018).

2.4 Synthesis Methods of Nanoparticles

The synthesis of Ag and Fe_2O_3 NPs can be done using top-down or bottom-up methods. Using methods like laser ablation and puttering, the top-down strategy entails reducing a bulk material

into nano-sizes. The term "bottom-up approach" refers to the process of creating nanoparticles from smaller components, such as chemical and biological processes (Alharbi, Alsubhi, and Felimban 2022). In the past, scientists have created nanomaterials by chemical or physical processes such the sol process, micelles, chemical precipitation, hydrothermal technique, pyrolysis, and chemical vapor deposition. The synthesis of AgNPs, like for most nanomaterials, is mainly divided into three Different processes: chemical, physical and biological synthesis (Abdulsahib, 2021).

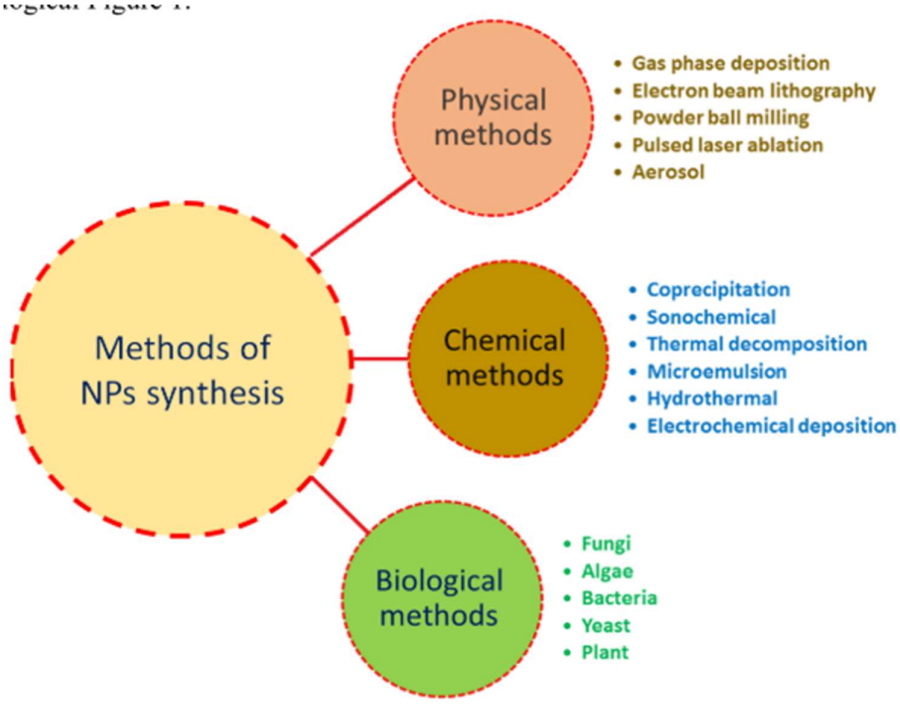

Figure 1. Schematic illustration of the production of nanoparticles via several processes.

2.4.1 Physical methods

The use of physical methods allows the synthesis of nanoparticles in the absence of solvent, permitting the uniformity of Ag and Fe_2O_3 NPs size distribution compared to chemical routes. The physical method for nanoparticles synthesis are Evaporation-condensation, Laser ablation, Thermal decomposition, Ultrasonic spray pyrolysis and Arc discharge method (De Matteis *et al*., 2018).

The physical methods consist of “top-down” and “bottom-up” approaches. In the top-down approach, the bulk materials are broken into nano-sized particles i.e., through high energy ball milling. It is difficult to obtain NPs of desired shape and size through mechanical crushing.

While in bottom-up approach, the well- dispersed and fine nano-scaled tiny particles can be obtained than the top-down approach. The example of bottom-up approach is laser evaporation. Some other physical methods like wire explosion method and inert-gas condensation method are also used to prepare MNPs (Ali *et al*., 2021).

2.4.2 Chemical methods

Essentially, chemical reactions require metallic precursors, reducing agents, and stabilizing/capping agents. During the reduction in silver salts, nucleation occurs after the NPs rise. For the production of stable NPs, chemo-reduction is the technique that is most frequently used. The dangerous substances used in the manufacture of Ag NPs include elemental hydrogen, ascorbate, citrate, borohydride thio-glycerol, and 2-mercaptoethanol. Due to the potential for chemicals to condense on their surfaces, the purity of the produced NPs is also lower than anticipated. Ag and Fe_2O_3 NPs preparation could be difficult, necessitating an additional step to prevent particle aggregation. Additionally, throughout the synthesis process, too many toxic and hazardous byproducts are eliminated (Zahoor *et al*. 2021).

2.4.2.1 Sol-gel methods

Widely used in the creation of nanomaterials is the wet chemical procedure known as the sol-gel method. A range of superior metal-oxide-based nanomaterials are produced using this approach. In addition to being affordable, the sol-gel method has a number of other benefits, including as the homogeneous nature of the material produced, the low processing temperature, and the ease with which composites and complex nanostructures can be made (Salem *et al*., 2022). It is common practice to synthesize metal and metal oxide NPs at low temperatures using the sol-gel technique, a colloidal chemistry technology. Materials' monomers are transformed into colloidal solutions (sols) in the first stage, which serve as the building blocks for the production of gels, which in turn give rise to particles or polymers. To obtain colloids, the precursors are hydrolyzed and polycondensed(De Matteis *et al*., 2018). The sol-gel method is a conventional and industrial method widely used for the synthesis of various NPs , offering, especially, good control over their size, high purity and homogeneity and low temperatures (on the downside, the use of organic solvents, availability of necessary precursors and long reaction times pose challenges)(Negrescu *et al*., 2022).

The sol-gel method is a wet chemical strategy that is frequently used in the creation of nanomaterials. A number of products are made using this method. Sol-gel is an in-situ technique that works well for regulating particle shape and size. It fundamentally entails the creation of a sol followed by its gelation and is made up primarily of condensation and hydrolysis processes. As precursors, metal alkoxides or organic and inorganic salts may be utilized (Baoum & Amin, 2021). For the creation of ceramics and nanocomposites (mainly oxides), sol-gel is one of the straightforward wet chemical processes that is frequently utilized. The sol-gel process is a chemical conversion of a sol into a gel (three-dimensional polymer) state, followed by a transition into solid oxide material due to the application of the proper post-treatment. This method is based on inorganic polymerization reaction including hydrolysis, polycondensation, gelation, aging, drying, and calcination or sintering (densification) (Hujjatul Islam *et al*., 2019).

The sol-gel method (wet-chemical approach) is a combination of condensation and hydrolysis reactions between iron alkoxides and salts (such as chlorides, nitrates, and acetates). The key benefit of this technology is the high purity, quantity, and good uniformity of IONPs. The method's drawbacks include the need for precise compliance with pH, temperature, and reagent concentration values during a synthesis; the expensive cost of precursors; and the low wear resistance of manufactured IONPs (Gudkov *et al*., 2021).

2.4.2.2 Solution combustion synthesis methods

Professor K.C. Patil invented the solution combustion technique first. It is one of the wet chemical processes that uses an exothermic reaction between metal nitrates (oxidants) and an organic fuel. The fuel needs to have carbon and hydrogen, which when burned produce CO_2, H_2O, and heat. The majority of metal oxides may be produced by mixing a metal, nitrate, and fuel. Because they offer a metal ion that is water soluble and promotes higher homogeneity, nitrates are used as the metal precursor. The temperature, fuel-oxidant ratio, and precursor chemical make up the solution combustion process' primary control parameters. One of the most crucial factors affecting the characteristics of the combustion-produced nanopowders is the fuel-oxidant ratio (Rane *et al*., 2018). For the preparation of oxide materials with controlled properties (high purity and homogeneity) for a variety of applications, including catalysts, solid fuel cells, and electronics, solution combustion synthesis is a quick, easy, efficient, and adaptable method that is gaining popularity across the globe. The chemistry of propellants and

sol-gel are the origins of SCS, although SCS is quicker than sol-gel and can produce products of superior quality. The metal precursors are the source of the metal cations in the solution combustion synthesis, thus determining the final metal oxide. The metal precursor are typically salts and can have three types of counter anions groups: oxidants, reducers or neutrals(Carlos *et al*., 2020).

2.4.2.3 Chemical reduction

The most common chemical method is chemical reduction, which allows for the synthesis of silver-iron oxide nanocomposite in solutions (water or organic solvents) in the presence of (i) metal precursors, (ii) reducing agents' sodium citrate, ascorbate, sodium borohydride (NaBH4), elemental hydrogen, polyol process, Tollen's reagent, N, N-dimethylformamide (DMF), poly(ethyleneglycol) (De Matteis *et al*., 2018).

2.4.3 Biological methods

The green synthesis uses extracts from the different plants as a source of capping and reducing agents in the preparation of Ag and iron oxide nanocomposite; it is suggested that the bio-molecules, especially secondary metabolites in those extracts, could reduce the Ag ions. They consist of vitamins, polysaccharides, amino acids, proteins, enzymes, polyphenolics, flavonoids, and other secondary metabolites. Likewise, proteins found in the plant extracts also play an essential role as a reductant of the Ag^{+} and as a size controlling agent for the formulation of AgNPs. Functional groups such as carboxylic (COOH) found in glutamine and aspartic residues and OH group of the tyrosine residues are considered responsible for stabilizing Ag ion and producing small nanoplates of Ag with a little polydispersity (Zahoor *et al*., 2021).

Biosynthesis of silver nanoparticles is a bottom-up approach that mostly involves reduction/oxidation reactions. It is majorly the microbial enzymes or the plant phytochemicals with antioxidant or reducing properties that act on the respective compounds and give the desired nanoparticles(Prabhu & Poulose, 2012). The drawbacks of this approach include the need to use high concentrations of plant extracts that are deficient in bioactive molecules. To put it another way, the chosen plant may not contain sufficient amounts of bioconstituents, which act simultaneously as a reducing, capping, and stabilizing agent. Therefore, in order to

avoid the development of undesired oxide's nanomaterials, it is necessary to alter the reaction's environmental parameters, such as pH, temperature, duration, and in some cases, nitrogen gas. A suitable and practical characterization technique must first be developed in order to conduct an examination and identify the type of resultant nanomaterial (Al-Hakkani *et al*., 2021).

2.5 Characterization Techniques of Nanoparticles

2.5.1 X-ray diffraction (XRD)

X-ray diffraction (XRD) is a well-liked analytical technique that has been used for the analysis of both molecular and crystal structures, qualitative identification of various compounds, and quantitative resolution of chemical species, measuring the degree of crystallinity, isomorphous substitutions, and particle sizes. This technique has been applied to samples from a variety of scientific fields, including geological, polymer, environmental, pharmaceutical, and forensic sciences, to quantify phase identification, conduct quantitative analysis, and identify structural defects. Bragg's law is the X-ray diffraction's guiding principle. Typically, XRD relies on the wide-angle elastic scattering of X-rays. Although XRD offers many advantages, it also has several drawbacks, such as the difficulty in forming crystals and the ability to only obtain findings for a specific conformation or binding state. Another drawback of XRD is the low intensity of diffracted X-rays compared to electron diffractions(X.-F. Zhang *et al*., 2016).

2.5.2 Fourier transform infrared (FTIR) spectroscopy

FTIR spectrometer for infrared light. When analyzing functional groups, structural structure, and chemical bonding in organic and inorganic samples, FTIR spectroscopy creates an infrared absorption spectrum (Perklin Elmer Spectrum 100) (Shehzad *et al*., 2018). Accuracy, reproducibility, and a good signal-to-noise ratio are all things that FTIR can offer. It is more common in academic and industry research to utilize FTIR spectroscopy to determine whether biomolecules are involved in the creation of nanoparticles. Additionally, FTIR has been used to analyze nanoscale materials, including the verification of functional molecules covalently grafted onto silver, carbon nanotubes, graphene, and gold nanoparticles, as well as interactions between enzyme and substrate during the catalytic process. It is also a non-invasive procedure. Finally, quick data collection, a strong signal, a high signal-to-noise ratio, and less sample heating up are benefits of FTIR spectrometers over dispersive ones. In order to determine the

function of biological molecules in the reduction of silver nitrate, FTIR is a suitable, useful, non-invasive, economical, and straightforward approach (X.-F. Zhang *et al*., 2016).

2.5.3 Scanning electron microscopy (SEM)

SEM is a surface imaging technique that is completely able to resolve various particle sizes, size distributions, forms of nanomaterials, and the surface morphology of the generated particles at the micro and nanoscales. We can examine the morphology of particles using SEM and generate a histogram from the images by manually counting and measuring the particles or by utilizing specialized software. SEM has the drawback of being unable to resolve interior structure, but it is still capable of giving useful information on purity and particle aggregation levels. Modern high-resolution SEMs can recognize the morphology of nanoparticles that are less than 10 nm (Zhang *et al*., 2016). The size and morphology of Ag and Fe_2O_3 NPs were investigated using JEOL-6490A-JSM scanning electron microscope (SEM)(Shehzad *et al*., 2018).

2.5.4 UV-Visible Spectroscopy (UV-vis)

The absorption spectrum of the reaction mixtures was re- corded at room temperature using UV–Vis spectrophotometer (Rayleigh, UV-2100) at a resolution of 1 (Ghaffari-Moghaddam & Eslahi, 2014). Both UV and visible emissions are common in metal oxide semiconductors; the UV emission corresponds to the near band edge emission and is caused by free-exciton recombination, while the visible emission is caused by deep-level emission due to impurities and various types of structural defects in the structures (Muneer & Farrukh, 2022).

2.5.5 Photo luminescence (PL)

Photoluminescence spectroscopy (PL) is a crucial method for figuring out the impurity levels in materials as well as the crystalline quality and optical band gap energy. The kind and concentration of defects, microstructure and morphology, size, and excitation wavelength all have a significant role in determining the peak position and relative peak intensity (Muneer & Farrukh, 2022). Photoluminescence (PL) is an important method for estimating semiconductor purity and crystallinity performance and disorder amount estimation present in the lattice structure. Photoluminescence has a wide variety of uses including energy band gap estimation,

level of impurities, and identification of defects, understanding of the mechanism of recombination, quality monitoring of materials, molecular structure, and modeling of the crystallinity(Al-Hakkani *et al*., 2021).

2.5.6 Thermogravimetric analysis (TGA)

TGA is an analytical technique used to determine the thermal stability of a material. The fraction of the volatile components present in the material can also be determined by monitoring the weight change that occurs as the sample is heated(Hasan *et al*., 2015). Thermo gravimetric analysis (TGA) is employed to verify the temperature-dependent changes(Ponnaiah *et al.*, 2018). As a mass loss versus temperature increases, thermal analysis (TA) also known as thermal gravimetric analysis (TGA) is used to determine the chemical and physical properties of any sample (Al-Hakkani *et al*., 2021).

2.6 Application of Nanomaterials

Nanomaterials have a wide range of uses in the fields of medical, chemistry, environment, energy, agriculture, information, communication, heavy industries, and consumer products. Figure 2 shows some of the nanoparticles created by various metal solutions and some of their potential uses. Nanomaterials, in particular, offer enormous potential for use in the treatment of surface and groundwater, wastewater, and the remediation of contaminated sites (Devatha & Thalla, 2018).

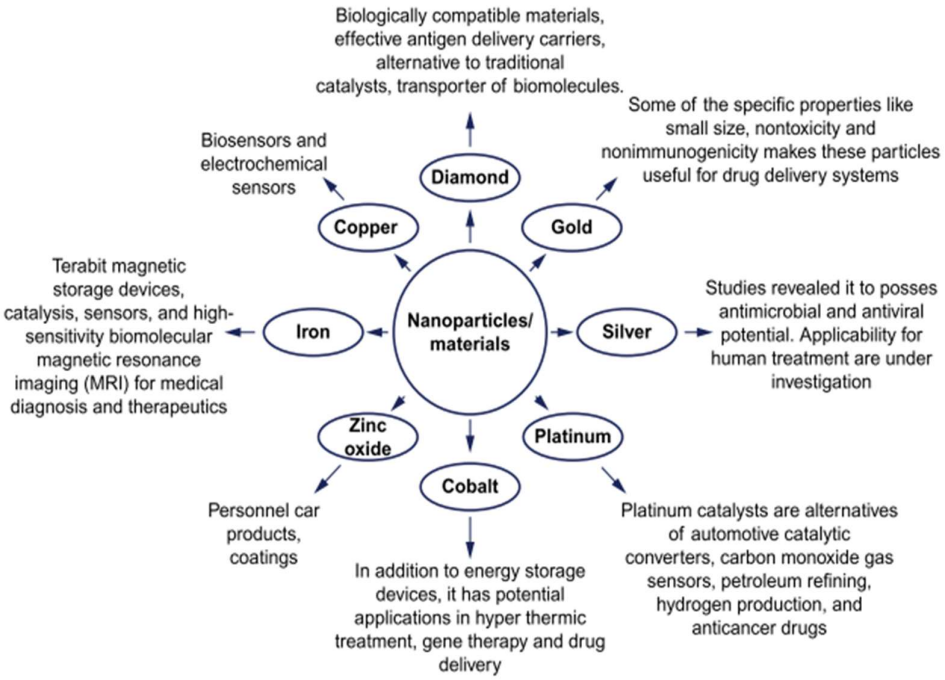

Figure 2. Applications of various metallic nanoparticles

2.6.1 Application of silver nanoparticles

Silver ions are a potent antibacterial and kill bacteria by interfering with their thiol groups, which are found on many crucial bacterial enzymes and proteins. Due to its unique toxicity to germs while still posing a low risk to humans, silver has been used in a broad variety of products, including bandages, packaging, and anti-fouling surface coatings. Silver nanoparticles function as an efficient antibacterial agent because they are a source of silver ions with a large surface area. When oxygen and protons are present, the particles in an aqueous environment oxidize, dissolving the particle surface and releasing Ag ions. Silver nanoparticles' long-term antibacterial activity is based on their ability to maintain an effective concentration of silver ions in a wide range of diverse solutions(Oldenburg, 2019). Silver nanoparticles may be of promising help in this struggle as they effectively eliminate bacteria at relatively low concentrations of silver nanoparticles; concentrations that are not toxic for human cells. antibacterial activity of silver nanoparticles depends on their size(Prucek e*t al*., 2011). Generally, it is widely accepted that the main antibacterial effect of Ag NPs or Ag NPs-based materials is due to its partial oxidation and release of silver ions (Ag^{+}). After this oxidation occurs, the following actions can happen either simultaneously or separately: (1) uptake of free Ag^{+} followed by disruption of ATP production and DNA replication; (2) Ag

NPs and Ag^{+} interaction with bacterial proteins, disrupting protein synthesis; (3) Ag NPs directly damage cell membranes, interacting with the peptidoglycan wall cell and the plasmatic membrane causing cell lysis(Domènech *et al*., 2013).

The antibacterial properties of silver have been recognized over 2,000 years ago. In general, Ag nanoparticles are effective. against many bacteria and can destroy 650 types of bacteria, viruses and fungi due to enhancement of antibacterial, antiviruses, and antifungal activity of Ag at the nano scale even around 100%. These nanoparticles are more sustainable, efficient and simple to process when compared with other antibacterial agents(Ghaffari-Moghaddam & Eslahi, 2014). Even in its ionic state, nanotechnology has created countless opportunities for water purification. Many different nanostructured materials have been developed, and they offer qualities including high aspect ratio, reactivity, controlled pore volume, electrostatic, hydrophilic, and hydrophobic interactions that are helpful in adsorption catalysis, sensing, and optoelectronics. Silver, titanium, gold, and iron nanoscale metals and their oxides have been extensively employed in environmental mitigation. Ag-NPs effectively eliminate biological pollutants such bacteria, viruses, and fungus (Salem *et al*., 2022). Many recent aspects of studies have included the use of gold, silver, and iron NPs/NMs to be used by Gram- positive and Gram-negative bacteria as a wide spectrum antibiotic. Studies have also been developed and applied to include the use of such Ag-Fe_2O_3 NPs as an antifungal for different organisms(Al-Hakkani *et al*., 2021). The little-sized nanoparticles with a vast surface range to volume proportion give a more effective intends to antibacterial action even at low fixation. Additionally, the antimicrobial action of silver nanoparticles relies on the fixation and shape. The main advantages of the silver nano coatings are Environmentally friendly, Harmless to skin, Easy handling, Breathability remains, Dry cleaning resistant, Ironing resistant, Suitable for all textiles, Long lasting sealing of textiles, Prevents tea, coffee and ketchup stains, Simply wash off contaminants, Washing stable up to 40°C, look, texture and breathability of the material remains, Long lasting protection for the textiles against dirt water and grease(Abbas *et al*., 2018).

2.6.2 Application of Fe_2O_3 nanoparticles

The iron oxide nanoparticles have a great attraction in biomedical applications due to their non-toxic role in the biological systems. The iron oxide nanoparticles have both magnetic behaviors and semiconductor property which lead to multifunctional biomedical applications. The iron

oxide nanoparticles play a major role in different applications, such as magnetic, electrochemical, gas sensor, energy storage, cancer therapy and magnetic storage, and biomedical treatments. Among the different types of nanoparticles, hematite (iron oxide) is one of the most common, natural and environmental-friendly(Sangaiya & Jayaprakash, 2018).

Iron oxide nanoparticles are currently used as contrast agents in magnetic resonance imagining (MRI) investigations. Another possible application of magnetic iron oxide nanoparticles fastens in the field of hyperthermia cancer treatments where hysteresis looses of magnetic nanoparticles generated during their cyclic remagnetizations under applied alternating magnetic fields are exploited to destroy cancer cells and tissues(Prucek *et al*., 2011). Due to their non-toxic, biodegradable and cheap nature, Fe_2O_3 NPs have been extensively studied as potential candidates for different cancer therapies. Data found in the literature indicate that Fe_2O_3 NPs are capable of killing tumor cells without affecting normal healthy tissue due to the increased in vivo sensitivity of tumors to heat damage. This allows the use of a specific cancer therapy called hyperthermia, where magnetic NPs can target tumors in a heat-specific manner through the alternation of fields, hysteresis and frictional heating(Negrescu *et al*., 2022). Over the last three decades, where traditional pharmaceutical methods have been widely used for antibacterial and antifungal therapies. This allowed these microorganisms to mutate and reproduce the new medium to continue with its adaptability and life. But, to combat the current conventional therapies, these microorganisms are in continuous production on their own. Scientists researching solutions thus have to actively study for best and safer ways to suppress and remove these microorganisms in their new type. Many recent aspects of studies have included the use of gold, silver, and iron NPs/NMs to be used by Gram- positive and Gram-negative bacteria as a wide spectrum antibiotic. Studies have also been developed and applied to include the use of such Fe_2O_3 NPs as an antifungal for different organisms(Al-Hakkani *et al*., 2021).

2.6.3 Application of Ag-Fe_2O_3 nanocomposite

The combination of surface properties of silver nanoparticles and magnetic properties of iron oxide nanoparticles leads to many potential applications, such as in biological targeting, separation and recovery, and catalysis, and the possibility of vectorized treatment with high levels of accumulation in the target tissue or specific target organ (Demarchi *et al*., 2018). The combination of magnetic properties of iron oxide nanoparticles and antibacterial features of

nanosilver thus predestinates these nanocomposites to be possibly used in disinfection and biomedical applications where they can be exploited for a targeted transport of an antibacterial agent and its subsequent removal by means of an external magnetic field(Prucek *et al*., 2011). The characteristics of both metals are obtained by combining Ag and Fe_2O_3. Because of these characteristics, scientists have been interested in creating an Ag-Fe_2O_3 hybrid composite with improved catalytic, bactericidal, and bio-imaging properties. Different methods, including physicochemical, chemical, and green synthesis using plant, algae, fungal, and bacterial extracts, can be used to create metal nanoparticles (Al-Zahrani *et al*., 2022).

2.7 Antibacterial Application of Ag-Fe_2O_3 Nanocomposite

Ag^+ ions from Ag/Fe_2O_3 nanocomposite highly interacts with the negatively charged components of DNA (phosphorus and sulphur) that lead to breakdown of both strands of DNA, distortion and morphological alterations of bacterial cell membranes and cell walls followed by cell death. Therefore, it is expected that better antibacterial activity might be due to the combined effect of Fe_2O_3 and Ag of Ag-Fe_2O_3 nanocomposite. There is different mode of actions of silver ions in terms of antimicrobial activity, such as (i) Interact with the respiratory mechanism, (ii) Inhibiting enzymes upon Ag ions interaction with the thiol group, (iii) Interfere with DNA replication after interacting with phosphate group, (iv) Interrupt cellular transport system after K^+ depletion (v) Disruption of cell membrane after contact of Ag nanomaterial (vi) Creation of reactive oxygen species (ROS). When the levels of ROS overawed the scavenging capability of microbial cell, they cause injury to cell membranes of bacteria, DNA and protein. The Ag-Fe_2O_3 nanocomposite also showed significant activity in both gram positive and gram-negative strains(A. U. Khan *et al*., 2020). Ag-Fe_2O_3 has an antibacterial impact on bacteria because it damages cell walls, disrupts structural proteins, inactivates enzymes, inhibits electron transport chains, damages nucleic acids (DNA), and causes oxidative stress brought on by the generation of reactive oxygen species (Al-Zahrani *et al*., 2022).

3. MATERIAL AND METHODS

3.1. Chemicals and Instruments

3.1.1. Chemicals and reagents

The chemicals and reagents required for the preparation of stabilized polymer silver-iron oxide nanocomposite and the antibacterial test were silver nitrates (AcrosOrganics), distilled water, polyvinyl alcohol (Sigma – Aldrich; 87-88% hydrolyzed, Mw =13000 – 23000 mol-1); ferric nitrate (Sigma-Aldrich), the bacterial strains, (*Staphylococcus aureus*(ATCC25923) and *Streptococcus Pyogenes(*ATCC19615)) and (*Escherichia coli* (ATCC25922) and *Pseudomonas aeruginosa (*ATCC27853)), bacteria used for checking antibacterial activity were taken from Adama Science and Technology University in Applied Biology Department, Muller Hinton agar (MHA) media for bacterial growth on the Petri-dish, ciprofloxacin and dimethyl sulfoxide (DMSO) were used. All the chemicals and reagents used for the preparation of silver-iron oxide nanocomposite were purchased commercially from local chemical markets. All those chemicals were used without any further purification.

3.1.2. Apparatus

The apparatus and instruments were used include furnace, aluminum foil, spatula, electronic beam balance, beaker, magnetic stirrer with hot plate, petri-dish, measuring cylinder, mechanical shaker, Erlenmeyer flask, refrigerator, mortar and pestle, beaker.

3.2 Experimental procedure

3.2.1 Synthesis of silver and iron oxide (Fe_2O_3) nanoparticles

A sol-gel combustion method was employed for the preparation of silver nanoparticles. 50 mL of distilled water was taken in a beaker. Then, the sample has stirred at 70 ℃ for 15 min, then added 1g of PVA, stirred the PVA solution up to gel formation (white color), then cool the prepared solution. Then, added 2.12 g of silver nitrate precursor and stirred for 1 hr. (when the precursor was added to the PVA solution had no color change). After that the prepared sample has been heated in oven at 110 ℃ for 8 hrs. Lastly the NPs were allowed to dry and ground so as to be used for further analysis. The iron oxide NPs also synthesized by the sol-gel combustion approach as reported in previous work (Gao *et al*., 2016),(Khort *et al*., 2021). with slight modifications such as adding surfactant as a stabilizing agent. A sol-gel combustion

method was employed for the preparation of Fe_2O_3 nanoparticles with same as AgNP except addition of 5.024 g of ferric nitrate precursor and calcined at 500 ℃ for 3 hrs.

3.2.2 Synthesis of Ag-Fe_2O_3 nanocomposites (SICs)

The SICs was also synthesized using the same approach as in section 3.2.1, except with the addition of appropriate amounts of the silver salt precursors silver nitrate in addition to the iron precursor ferric nitrate. The amount of dopant (taking the difference percentage of dopant/host percentages) was optimized. The optimized percentage of host metal was listed in table below. After preparation the powder was dried at 110 ℃ in oven for 8 hrs. and then calcined 500℃ for 3hrs in furnace.

Table 1.Amount of different percentage of precursor

Sample (%)	Concentration (M)	$AgNO_3$ (g)	Sample (%)	Concentration (M)	(Fe $(NO_3)_3 \cdot 9H_2O$) (g)
100(Fe_1)	0.25	2.12	100	0.25	5.05
0.5(Fe_2)	0.00125	0.0106	99.5	0.24875	5.024
1(Fe_3)	0.0025	0.0212	99	0.2475	4.995
5(Fe_4)	0.0125	0.106	95	0.2375	4.7975
10(Fe_5)	0.025	0.212	90	0.225	4.545
15(Fe_6)	0.0375	0.32	85	0.2125	4.2925

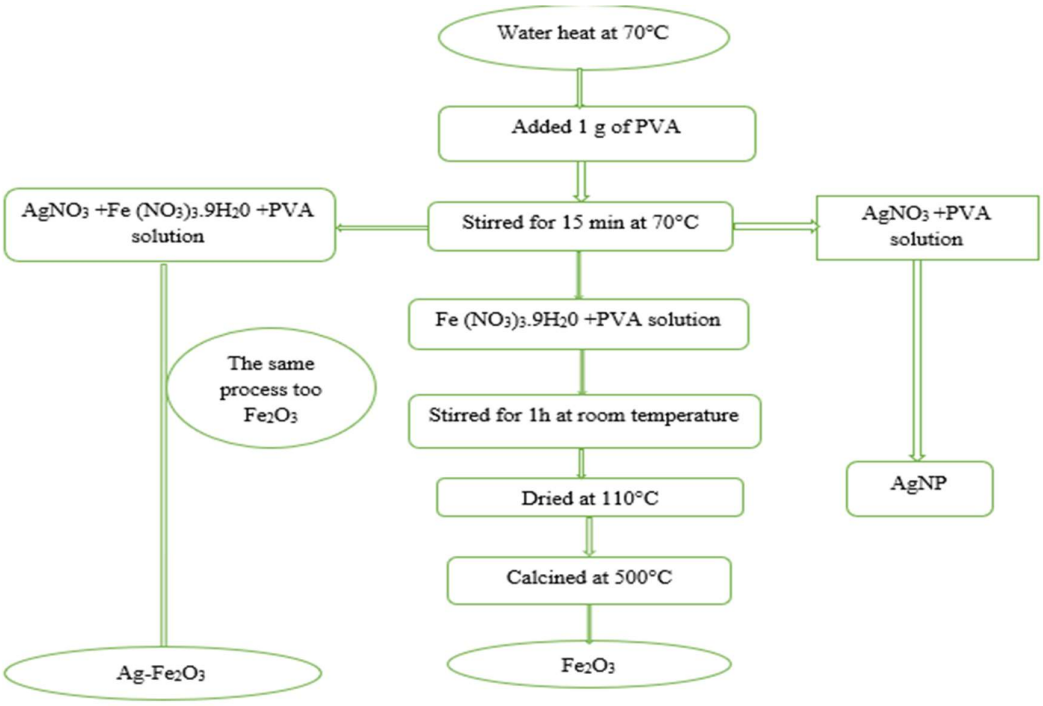

Figure 3. Flowchart for the synthesis of Fe_2O_3 nanoparticles and SICs by sol-gel combustion method.

3.3 Characterization

Different characterization techniques were performed to know the crystalline structure, optical properties and morphology of synthesized nanoparticles and nanocomposite. The detail procedures are mentioned below for each technique. all characterization technique performed based on XRD result that have small crystalline size.

3.3.1. Thermo Gravimetric analysis (TGA)

The thermal behavior was evaluated by Thermo Gravimetric (TGA) and Differential Thermal Analysis (DTA) in the air using DTG-60 detector. As indicated in numerous works concerning PVA polymer or PVA-metal oxide composite, an optimum temperature of 300 - 500 °C is suitable to remove the PVA after its role as capping agent and unwanted impurities (Abd-Elrahman, 2013; Ghafari *et al*., 2017; Radhamani *et al*., 2016).

3.3.2.X-ray diffraction (XRD)

The XRD analysis used to study the crystalline structure of the synthesized nanoparticles and nanocomposite samples. For all samples their Powder were used in analysis. XRD works by irradiating a material with incident X-rays and then measuring the intensities and scattering angles of the X-rays that leave the material. The XRD analysis (2θ scan) was performed using an X-ray diffractometry (XRD700, Shimadzu Co., Japan). The diffraction data were recorded within a range of 2θ from 10° to 80° for Ag and Fe_2O_3 NPs and SIC. The diffraction data were recorded at 40 kV and current of 30 mA in continuous scan mode with scan rate 3 (deg/ min) by using Cu-Kα radiation with a wavelength of 1.5406 Å. The average crystallite sizes (D) of the powders were calculated by using Debye-Scherrer's formula, $D = K\lambda/(\beta \cos(\theta))$, Where, λ is the X-ray wavelength, θ is Bragg's diffraction angle, and β is the Full width at half maximum (FWHM) of the diffraction line at half of the maximum intensity. The different crystalline phases in the samples were identified by comparing the data with the Joint Committee for Powder Diffraction Standards (JCPDS) files.

3.3.3. UV–Vis diffused reflectance (UV–Vis DRS) spectroscopy

Diffuse reflectance spectra were obtained in a spectrophotometer model (UV3600plus, Shimadzu, Japan), with a coupled integration sphere. The spectra were obtained for powder samples in the wavelength range of 200 – 800 nm. The reference was a 100% reflectance sample.

3.3.4. Fourier transform infrared (FT-IR) spectroscopy

Fourier transform infrared (FT-IR) spectroscopy helps to ascertain the identity of various Phyto-chemical constituents involved in the reduction and stabilization of the nanoparticles and nanocomposites. FT-IR spectrum for dry powders of Fe_2O_3 NPs and 15 SIC was obtained using Perkin Elmer FT-IR Spectrophotometer Frontier in the range of 4000–400 cm^{-1}.

3.3.5. Morphological and composition characterization

Scanning electron microscopy with energy-dispersive x-ray spectroscopy (SEM-EDX-EVO18 model with low vacuum facility and ALTO1000Cryo attachment) was used for understanding morphological and structural features of Fe_2O_3 NPs and 15 SIC. SEM is a type of electron

microscope, its powerful technique for analyzing the structure of the prepared metal nanoparticles, which produces images of a sample by scanning it with a focused beam of electrons. The information about the sample's surface topography, morphology, and composition of the obtained metal nanoparticles was examined by using scanning electron Microscope(AL-Awadi *et al*., 2018).

3.4. Antibacterial Test

The antibacterial activity of Ag NPs, Fe_2O_3 NPs, and SICs were investigated against two Gram-negative *(Escherichia coli (*ATCC 25922)*),* and *Pseudomonas aeruginous (*ATCC 27853*)),* and two Gram-positive *(Staphylococcus aureus (*ATCC 25923)*), and Streptococcus Pyogenes (*ATCC 19615*))* using disk diffusion method in Applied Biology Department laboratory of Adama Science and Technology University. ciprofloxacin (25 µg) antibiotics and DMSO was used as positive and negative control respectively.

3.4.1. Disk diffusion methods

Muller Hinton Agar was prepared by dissolving, 38 g of Muller Hinton powder in 1L of distilled water separately and then sterilized by autoclave at 121 ℃ and 15-pound pressure for 20 min. After cooling, about 20 mL of medium are added aseptically to sterilized Petri dishes. Then the Petri dishes were labeled and incubate until they solidify.

Bacterial sub cultures were maintained on broth at 37 ℃. Bacterial strains were taken from Oromia regional laboratory, Adama and grown aerobically on broth for 24 h at 37 ℃. Bacterial suspension was prepared by taking it from broth and dissolving in sterile normal saline until the concentration of bacterial suspensions were achieved to 1×10^8 colony forming units (CFU) mL^{-1} by comparison with the 0.5 McFarland Standard. 100 µL of 24 hrs. standardized culture of test bacteria was first evenly spread onto the surface of the Muller-Hinton agar plates using sterile cotton swabs. A sterile swab is used to inoculate the surface of the media in Petri dishes making three rotations with an angle of 60° to ensure a homogeneous growth. The plates were then turned upside down. 100 mg of each prepared sample were dissolved in 1 mL DMSO (100 mg mL^{-1}). From 100 mg mL^{-1} concentration of each sample, 50 mg mL^{-1}, 25 mg $mL^{-1,}$ and 12.5 mg mL^{-1} were diluted serially for Fe_2O_3 NPs and 15 SIC and 0.5 SIC. 6 mm diameter disk were saturated with 20 µL of each concentration and 25 µg of ciprofloxacin (positive control) and

DMSO (negative control) placed on a plate covered with lids and incubated at 37 °C for 24 hrs. The diameter was measured from the area around the disk where no bacterial growth has been observed, called the inhibition zone. All antibacterial tests were carried out in triplicate and the averages were reported. This diameter can be compared to the critical diameters of antibiotics ciprofloxacin and images were captured. Fe_2O_3 NPs, 15 SIC, and 0.5 SIC were used for comparison.

3.5. Data Analysis

Data in the current study (antibacterial activity data) were analyzed by Microsoft Excel 2010 software. The means of three replications and standard error (± SE) were also calculated for all the results obtained. Differences between means were considered significant at P-values < 0.05. OriginPro 8, SysTools XPS Viewer, were also used to analyze the data.

4. RESULT AND DESSCUSION

Here we present the structural, morphological, and optical properties of Fe_2O_3 and 15SIC based on XRD results that had small crystalline size. The composite was characterized by TGA, XRD, UV-vis/DRS, FTIR, PL, and SEM-EDX. Antibacterial activities of Fe_2O_3, 15SIC, and 0.5SIC (for comparison) were also presented.

4.1 Synthesis of Ag-Fe_2O_3 Nanocomposite

Synthesized of Ag NPs was accompanied without color change. In the beginning, the color of the mixture of PVA and boiled distilled water was white then the aqueous solution of $AgNO_3$ was also white also after 1hr of moderate stirring at room temperature, and after drying in oven the color was not changed.

In the same manner in the synthesis of Fe_2O_3 NPs, the color of the solution was changed immediately after adding the precursor, which indicated the formation of colloidal Fe_2O_3 suspensions. The formation of light orange precipitate after heating the solution mixture confirms the formation of iron hydroxide. Moreover, the formation of Fe_2O_3 NP was confirmed by the formation of gray powder after calcination of that calcined at 500℃.

The sol-gel combustion synthesis of SICs has been carried out by adopting the reported procedure by (Gao *et al*., 2016). with minor modifications. Silver nitrate ($AgNO_3$) and ferric nitrate ($Fe(NO_3)_3 \cdot 9H_2O$) were used as a precursor for the sol-gel combustion synthesis of SICs using PVA. One of the goals of this study was to use stabilized polymer (PVA) for the preparation of nanomaterials. The polyvinyl alcohol, which belongs to the polymer, was chosen and used in this study for SIC synthesis. The synthesis of SICs was conducted by adding $Fe(NO_3)_3 \cdot 9H_2O$ and $AgNO_3$ as a precursor to the PVA solution until a gradual change in the reaction color was observed. After 1 hr. of stirring at 70 ◦C, the color of the reaction mixture changed from white to light orange. Such a change of color of the reaction mixture represents the formation of SICs by the PVA solution.

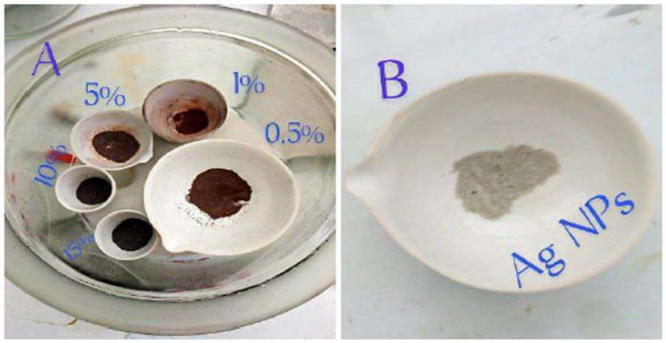

Figure 4.The color change of silver and silver-iron oxide nanocomposite in the synthesis process. A) SIC and B) silver NP.

4.2. Characterization

4.2.1. Thermogravimetric (TGA) analysis

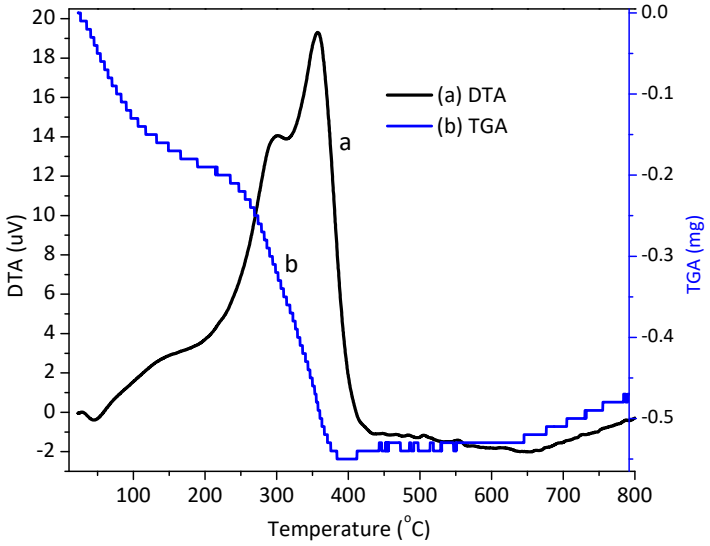

Figure 5. The TG-DTA thermal stability analysis: the TG-DTA plots of PAV-Fe_2O_3 NPs, respectively. At about 390 ° C, pure Fe_2O_3 NPs were obtained.

Figure 5 shows the TGA result of PVA-Fe_2O_3 NPs, In the thermal analysis study of PVA-Fe_2O_3 composites before calcination, at about 80-190 °C, the surface and interstitial absorbed water molecule evaporation and slow intramolecular decomposition occurs. Within the PVA melting point range of 230°C - 410 °C, the degradation of its amorphous part and the intermolecular decomposition were occurred (Abd-Elrahman, 2013; Kumar *et al*., 2019). The crystalline part of PVA decays at 398 °C (Radhamani *et al*., 2016; Rahmanian *et al*., 2015), and complete

decomposition to yield carbon and hydrocarbons that results in the liberation of CO_2 gas and pure Fe_2O_3 phase happens at about 400 °C (Ghafari *et al*., 2017; Mallakpour *et al*., 2015; Radhamani *et al*., 2016). Moreover, increasing the annealing temperature can also enhance the aggregation of metal oxides.

4.2.2. X - ray diffraction (XRD) result analysis

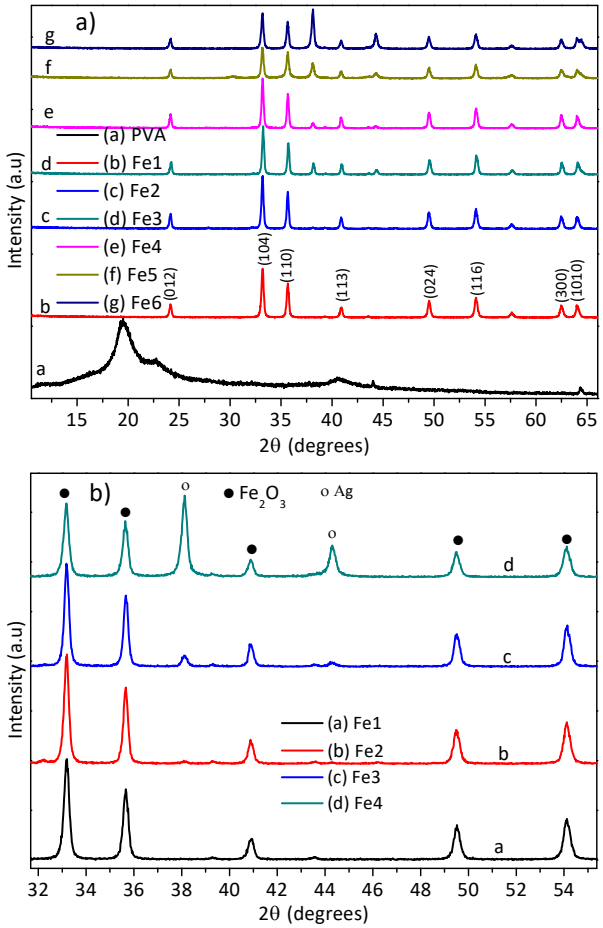

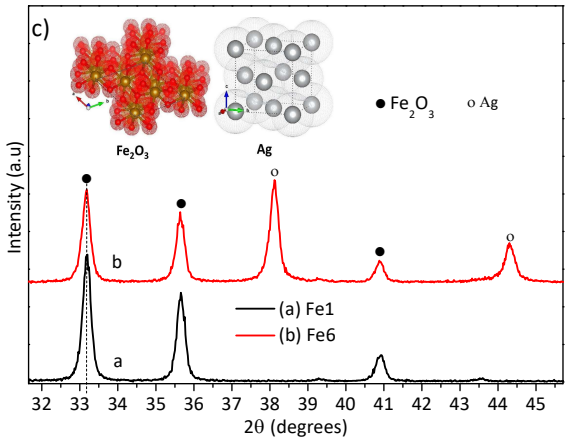

Figure 6. XRD pattern of PVA, Ag, Fe_2O_3 NPs, and SICs nanocomposites: (a) XRD patterns of Fe_2O_3 and different percentages of SIC, (b and c) Magnified view XRD pattern for Fe_2O_3 and SICs; there is no higher or lower angle shift on the XRD pattern of the composites than single Fe_2O_3, confirming the non-inclusion of silver in the Fe_2O_3 lattice. The inset in Fig. 6c is the structure models of Ag and Fe_2O_3 NPs. crystals developed by the software 3D Visualization for Electronic Structural Analysis (3D-VESTA) from the crystallographic information file (CIF) data.

The average crystallite sizes and crystallinity of synthesized PVA, NCs, and NPs were analyzed from the XRD pattern analysis (Fig. 6a-c). The PVA polymer precursor before calcination showed abroad semi-crystalline peak at 19.2 degrees, which corresponds to the (101) crystal plane (JCPDS, 00-053-1847)(Selvi *et al*., 2019). According to figure 6a(b), single Fe_2O_3, the diffraction angles with their corresponding crystal planes (~24° (012), 33° (104), 36° (110), 51° (024), 54° (116), 62° (214), and 64° (300)] are indexed to hematite, α-Fe_2O_3 (JCPDS: 00-033-0664, R-3c (#167-1) space group)).

The XRD diffraction spectrum of sol-gel combustion synthesized in, 1, 5,10 and 15SIC respectively, shown in Figure 6(a(d-g)), which demonstrates a total of eight major peaks, ranging from 10° to 80°, the peaks at 2θ values of 24.18°, 33.19°, 35.67°, 40.91°, 49.51°, 54.11, 62.48 and 64.04 and corresponds to hkl plane in a crystal lattice i.e., (012), (104), (110), (113), (024), (116), (214) and (300) crystallographic planes, respectively. In addition to the diffraction peaks of α- Fe_2O_3, diffraction peaks of (111), (200), (220) and (311) planes of silver located at 2θ=38.17 °, 44.34 °,64.49 ° and 77.44 ° are observable, indicating successful silver embedded

to the surface of Fe_2O_3. For 0.5SIC, an independent peak for Ag was not detected, which is probably due its inclusion in the Fe_2O_3 lattice. However, a clear independent peak was detected for Ag in addition to Fe_2O_3 starting from 1SIC to 15SCI, and its intensity increased with increasing the amount of Ag. The relatively weak intensity of silver peaks can be attributed to coating of silver NPs by Fe_2O_3 studied in previous reported (Mirzaei *et al*., 2016). The XRD analysis confirms that the prepared sol-gel/combustion synthesized SICs showed lattice planes of face-centered cubic crystalline structure with no impurities within the XRD instrument's detection limits. In the case of SICs, the presence of similar prominent peaks of Fe_2O_3 and Ag metal indicates the formation of SIC. For all Composites, the observed peaks can be taken as confirmation of the formation of SICs. The absence of a higher or lower peak shift for 15 SIC (see Fig. 6c) compared to pure Fe_2O_3 indicates the absence of Ag dopant inclusion in the Fe_2O_3 host lattice and the dominance of Ag-Fe_2O_3 Schottky contact formation(Ansari *et al*., 2013) .

The XRD data and the respective crystallite size are calculated using Debye-Scherrer's formula ($D = K\lambda/(\beta \cos(\theta))$). Where λ is the wavelength of X-ray radiation (for Cu Kα 0.15418 nm), K is constant, β is the line width at half maximum height, and θ is the diffracting angle. Furthermore, the XRD pattern of sol-gel combustion synthesized SICs shows sharp and intense peaks, indicating that the prepared samples were finely ground, homogenized with high crystalline quality, and average bulk composition is determined. The (104), (110), (116) planes were chosen to calculate the crystallite size of Fe_2O_3 NP and SICs the average crystallite sizes from the XRD data.

Table 2.Crystallite size of Ag and Fe_2O_3 and Ag-Fe_2O_3

sample	Fe_2O_3(%)	Ag (%)	Average size(nm)
Fe_1	100	-	34.7
Fe_2	99.5	0.5	38.76
Fe_3	99	1	41.63
Fe_4	95	5	39.88
Fe_5	90	10	37.46
Fe_6	85	15	34.55
Ag	-	100	55.2

Table 3.Calculations of average particle sizes of and Synthesized NCs Samples

Sample	Peak position (2θ (°))	d(Å)	FWHM (°)	D(nm)	Average D(nm)	(hkl)
Fe_2O_3 NPs	33.19	2.69647	0.24760	35.08		(104)
	35.66	2.51515	0.25000	34.88	34.70	(110)
	54.11	1.69357	0.27220	34.23		(116)
0.5SIC	33.19	2.69689	0.2020	39.3		(104)
	35.66	2.51523	0.21150	41.2	38.76	(110)
	54.10	1.6937	0.26030	38.76		(116)
1SIC	33.2515	2.69224	0.21140	40.95		(104)
	35.7246	2.51133	0.20290	42.95	41.63	(110)
	54.1616	1.69205	0.22730	40.99		(116)
5SIC	33.2016	2.69617	0.2156	40.14		104)
	35.6769	2.51457	0.2124	41.025	39.88	(110)
	54.1148	1.69340	0.24190	38.		(116)
10SIC	33.1894	2.69713	0.23900	36.24		104)
	35.6597	2.51575	0.23690	36.81	37.46	(110)
	54.0960	1.69395	0.23690	39.34		(116)
15SIC	38.1217	2.35874	0.25400	34.58		(111)
	33.1824	2.69768	0.24960	34.38	34.55	(104)
	35.6579	2.51587	0.25360	34.7		(110)

4.2.3. UV-visible diffuse reflectance (UV-Vis - DRS) spectra and Bandgap Analysis

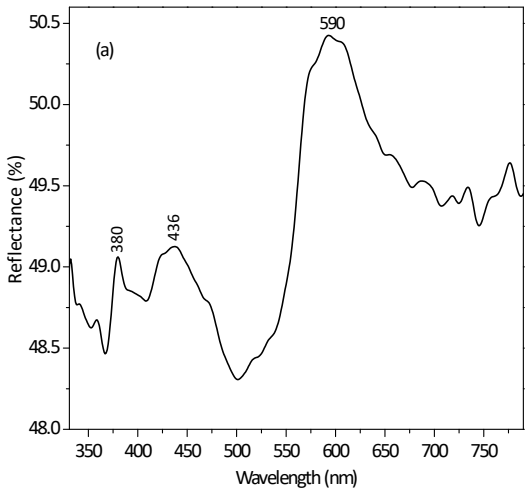

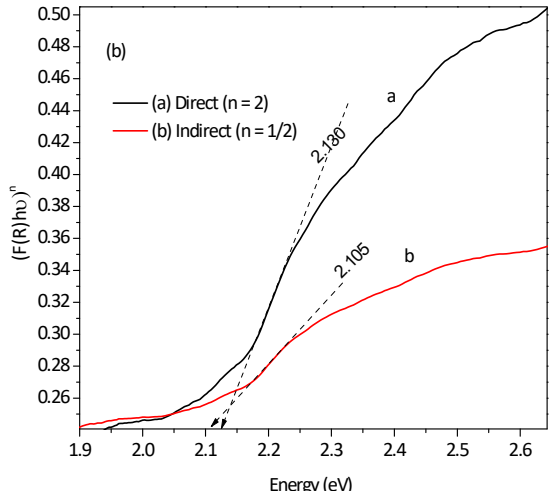

Figure 7. The UV-vis-DRS spectra of 15SICs materials: (a) The UV-vis-DRS spectra of 15SIC, (b) are the direct and indirect Kubelka-Munk (K-M) plots.

Figure 7 shows UV-vis-DRS spectra and direct and indirect bandgap energies of 15SIC. As shown fig. 7(a) Synthesized 15SIC shows maximum absorption peaks at 590 nm. This absorption peak was due to the strong surface plasmon resonance (SPR) band, these peaks depend on the particle size and shape of NPs. The change in the optical properties can be realized by the Kubelka-Munk function (Abebe *et al*., 2021) . The calculated direct and indirect bandgap values of 15SCI are found to be 2.13 and 2.10, respectively, which is smaller than the single Fe_2O_3 bandgap values reported in the literature (2.2-2.35 eV). This shows the slight inclusion of Ag in the Fe_2O_3 lattice, even if the Schottky junction between them is dominant.

4.2.4. Fourier transforms infrared (FT-IR) results analysis

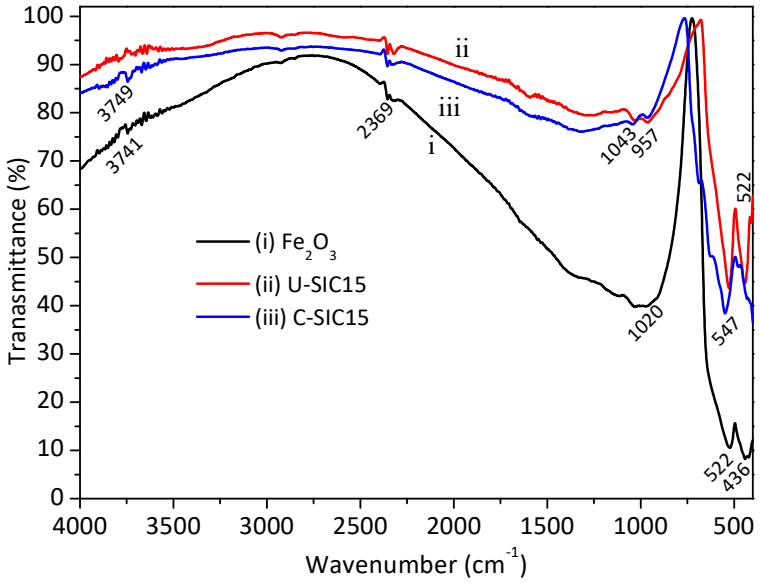

Figure 8. The FTIR spectroscopic chemical bonding analysis: the FTIR spectra of Fe_2O_3 NPs and 15SIC before and after calcination.

Metal-oxygen chemical bonding analysis for Fe_2O_3 and 15SCI (before and after calcination) was performed using FTIR techniques. According to Fig. 8(i-iii)., show the FTIR spectra of Fe_2O_3, and 15SCI (before and after calcination), the absorption bands are observed at 3741, 2369, 1043, 1020, 965, 957, 522, and 547, 444, 436 cm^{-1} etc... The common but short absorption band at about 3741 cm^{-1} is the result of absorbed water molecules. The peak below 1000 cm^{-1} is attributed to the longitudinal- and transverse-optical bending vibration modes of Fe-O or Ag-O bond(Anzlovar, 2015). The features at 522 and 436 cm^{-1} correspond to the metal–oxygen vibrational modes(Kayani *et al*., 2014). The slightly higher wavenumber shifts for calcined 15SCI than uncalcined 15SCI shows the rigidity of metal-oxygen as a result of condensation. The other peak detected at about 2369 cm^{-1} is probably from the precursors' intermediates. The major peaks at 547 cm^{-1} confirm the presence of Fe_2O_3 vibration compare to previous (Mishra *et al*., 2014).

Table 4.FTIR vibration frequency of Fe_2O_3 NPs and 15SIC before and after calcination.

Frequency (cm^{-1})	Bond stretching	Functional group
3741	O-H (strech)	alcohol
2369	C=O (stretching)	Carbonyl group
1043	C-O (strech)	Alkyl ketone
1020	C-O (strech)	Alkyl ketone
957	C=O(strech)	Alkyl ketone
547	C-X	Halo alkane
522	C-X	Halo alkane
436	C-X	Halo alkane

4.2.5. Photoluminescence result analysis

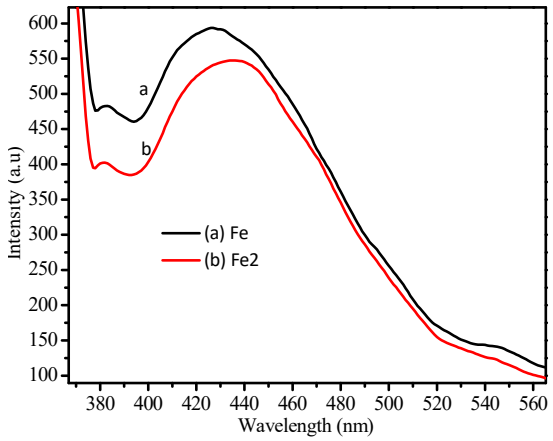

Figure 9. The photoluminescence (PL) spectra of Fe_2O_3 NPs and 15SIC materials: (a) The PL spectra of Fe_2O_3 and (b) PL spectra of 15SIC. A slight intensity reduction for the composites was observed compared to Fe_2O_3, indicating the presence of some electron-hole recombination hindrance due to doping.

Figure 9 shows the photoluminescence spectrum of Fe_2O_3 and 15SICs. The PL spectra of Ag-Fe_2O_3 composite synthesis by sol-gel-combustion methods at room temperature excited at 340 nm. This luminescence can be observed even with the naked eye at room temperature and is due to exciton emission(Lassoued *et al.*, 2018).The enhancement of the intensity can be related to the size of the nanoparticles, as the size increase the photoluminescence increases(Mathevula *et al.*, 2017). which have a greater intensity reduction for 15 SCI than that of pure Fe_2O_3. This intensity reduction for the 15SCI shows the presence of electron-hole recombination

diminishing properties. The slight blue shift for the composites over Fe_2O_3 is probably due to the Ag-independent peak(H. Khan *et al*., 2020).

4.2.6. SEM-EDX analysis

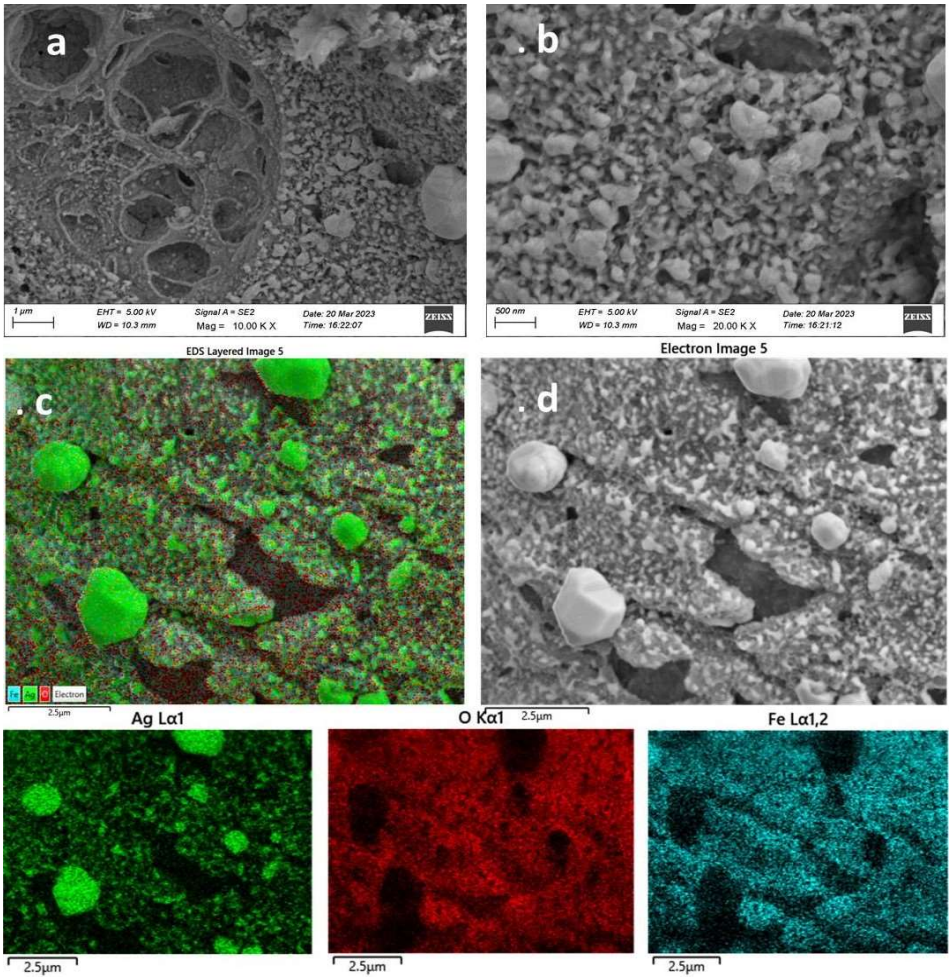

Figure 10.FESEM morphological and EDS elemental mapping analysis for 15SIC: (a) and (b) are the FESEM images for SICs at 1 µm and 500 nm magnifications, respectively. The porosity occurred was due to gas evolution. (c) The EDS layered image; (d) the FESEM image, from which the EDS mapping analysis was conducted. The green, red, and aqua images are the elemental mapping results for silver, oxygen, and iron, respectively. The good dopant elemental distribution on the Fe_2O_3 surface proves the potential of the sol-gel/solution combustion approach for synthesizing nicely distributed doped composites.

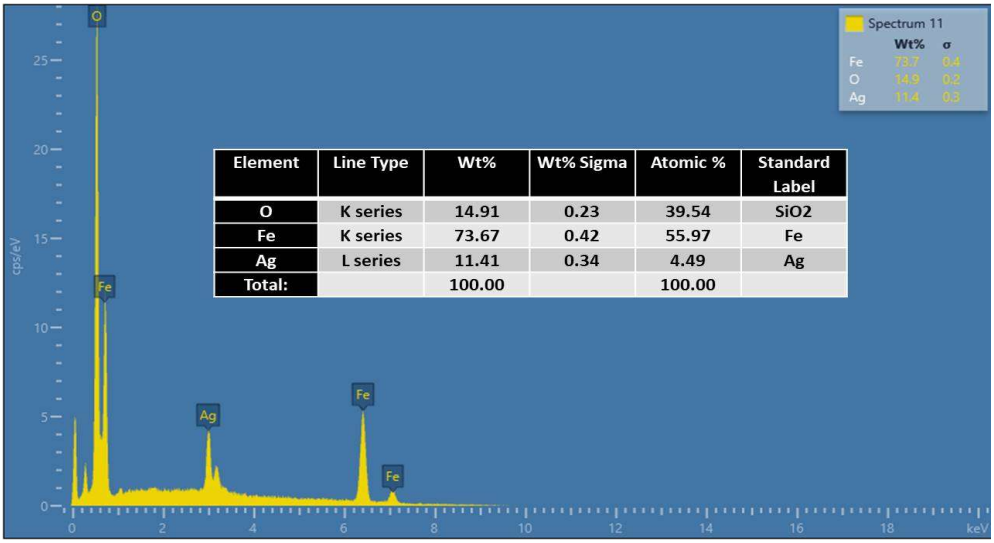

Figure 11. The EDX compositional analysis spectra for SICs show the presence iron, silver, and oxygen without any other impurities. The inset table in the EDX spectra shows the composition of the elements in the proportion for silver and iron, also in accordance with the precursor's amount taken during synthesis.

Figures 10 a and b shows the FESEM images of 15 SIC at two different magnifications of 1 and 500 nm, respectively. The image has porous morphology, which probably occurred due to the evolution of gas from many points during combustion(Abebe *et al*., 2022). The 15SIC seemed to have a mono-dispersed and aggregation-free micrograph. The EDX spectra revealed the existence of several well-defined peaks in the SICs that were due to silver, iron, and oxygen, components. Furthermore, EDX spectra revealed the production of a very pure 15SIC with no additional impurity-related peaks in addition, elemental EDX mapping was used to determine the Ag and Fe elemental distribution (spatial/lateral) of the 15SIC prepared. The mapping of Fe, Ag, and O elements has been shown Figure 11, Both Fe and Ag were uniformly distributed throughout the SICs sample, according to the EDX elemental analysis shown in the Ag, Fe, and O element mapping images of 15SIC. In previous studies reported, The appearance of main peaks around 3 keV and 6.5 KeV specify the elemental silver and iron as the main components(Ullah *et al*., 2020). The major peaks in which oxygen, iron, and silver are obtained on the EDX spectrum are at 0.5, 0.7, and 3 keV, respectively. The EDX measurement different area were focused both Ag and Fe_2O_3 can be seen in the synthesized composite in nanostructure in the EDX spectrum. The elemental percentage of 15SIC were found to be 55.97 % for Fe, 4.49 % for Ag and 39.54 % for O.

4.3. Antibacterial Activity Analysis

4.3.1. Antibacterial susceptibility test

The antibacterial activities of prepared NP and SIC was tested at applied biology laboratory against both the two gram-positive (*Staphylococcus aureus* ATCC25923 and *Streptococcus Pyogenes* ATCC19615) and two gram-negative bacteria *(Pseudomonas aeuruginosa* ATCC27853 and *Escherichia coli* ATCC25923*)* through the disk diffusion method. The standard ciprofloxacin (at 25 μg) has the antibacterial activities within the range of 21.6 ± 0.3 to 23.6 ± 0.3, 20.6 ± 0.6 to 23.3 ± 0.8, 23.3 ± 0.3 to 24.6 ± 0.3 and 20.3 ± 0.3 to 22.6 ± 0.3 for *E. coli, S. aureus, P. aeruginous and S. pyogenes* respectively. DMSO has no activity (6 mm) on whole tested bacterial strain and it was used as solvent in samples serial dilution.

Figure 12(a-c) illustrates photographs of the antibacterial tests results of synthesized samples and the details are summarized in Table (6). The presence of an inhibition zone indicates the antibacterial effect of the uncalcined Fe_2O_3 NPs, 0.5SIC and 15SIC. 15SICs the maximal SICs dose (100 g/mL) showed a high level of inhibitory activity against the pathogens, E. coli, P. aeruginosa, S. aureus and S.py with inhibition zones of 21.6, 22.6, 18.3 and 22 mm, respectively.

The antibacterial activity of sol-gel/combustion synthesized Fe_2O_3 NPs in four volume ratio was investigated against both the two gram-positive (*Staphylococcus aureus* ATCC25923 and *Streptococcus Pyogenes* ATCC19615) and two gram-negative bacteria *(Pseudomonas aeuruginosa* ATCC27853 and *Escherichia coli* ATCC25923*)* through the disk diffusion method. At 100mg/L The zone of inhibition values indicated that Fe_2O_3 NPs exhibited a varied range of 6.6-9.3 mm of antibacterial activities against (*Pseudomonas aeuruginosa and Escherichia coli*) (gram negative) the tested bacterial strains.

Figure 12(a). and Table 6). Shows In Fe_2O_3NPs, the range of zone of inhibition was between 7.6 ± 0.3 to 6.6 ± 0.3 mm and 9.3 ± 0.3 7.3 ± 0.3 for *Pseudomonas aeuruginosa and Escherichia coli*) respectively. A maximum zone of inhibition of 9.3 and 7.6 mm was produced against *Pseudomonas aeuruginosa and Escherichia coli*), respectively at the concentration of 100 mg/mL and 50mg/mL. No zone of inhibition was observed in *Staphylococcus aureus* and *Streptococcus Pyogenes* at all concentration. In comparison, the antibacterial activity of Fe_2O_3

NPs at 50 mg/mL, and 25 mg/mL and12.5mg/mL, were weaker than at 100mg/mL suggesting that the activity displayed has a dose-dependent manner (Table 6).

In figure 12(b) 0.5SIC showed the second most strong activity with a maximum zone of inhibition of 9.6, 9.6, 11.6, and 10.6 mm at the concentration of 100 mg/mL.9, 9.3, 9.3, and, 9 mm at the concentration of 50 mg/mL. 8.3, 8.3, 7.6, and 8.6 mm at the concentration of 25 mg/mL.7.6 ,6,7.3 and 7mm at the concentration of 12.5 mg/mL. against *S. aureus, P. aeruginosa, E. coli,* and *S. pyogenes,* respectively.

From the five of sol-gel combustion synthesized SICs 0.5SIC and 15SIC were checked, 15SIC showed better performance on the antibacterial activity as compared to Fe_2O_3 nanoparticle and 0.5SIC. In 15SIC the range of zone of inhibition was between 9.3-22.6 mm (Table 6). This could be due to the smaller average crystalline size and large surface area of NP properties. It indicates that the high antibacterial performance contributed due to the high ROS production. Then the high ROS production results from the use of PVA which contains amounts of OH radical. Silver particles have a good antibacterial effect on dangerous bacteria, whether they are Gram-positive or Gram-negative bacteria, according to an earlier study. In earlier studies, the antibacterial activity of Ag-Fe_2O_3 nanocomposite was examined, and it shown good activity against both Gram-positive and Gram-negative bacteria. Due to its negative effects on bacterial cell walls, disruption of structural proteins, inactivation of enzymes, inhibition of electron transport chains, destruction of nucleic acids (DNA), and induction of oxidative stress brought on by the production of reactive oxygen species (ROS), Ag-Fe_2O_3 has an antibacterial effect on bacteria. Ag/Fe_2O_3 has thus become an effective antibacterial treatment option and is helpful in the medical industry (Al-Zahrani *et al*., 2022). According to Ullah et al. (2020), the Ag-Fe_2O_3 nanocomposite's potent antibacterial activity may be a result of its sharp morphology and tiny size. In comparison to Gram-positive bacteria, the bactericidal impact of NPs was found to be similar but significantly stronger for Gram-negative bacteria. According to Santoshkumar et al. (2017), this is caused by the structural differences between Gram-positive and Gram-negative bacteria. Gram-negative bacteria have more complex cell walls than gram-positive bacteria, which serves as a permeability barrier for the absorption of ROS. Furthermore, gram-positive bacteria's membranes absorb negatively charged ROS species more readily than gram-negative bacteria's do (Gordon *et al*., 2011; Russell, 2003).

Table 5. Antibacterial activity of SICs sol-gel synthesized Fe_2O_3 NPs and 0.5SIC and 15SIC.

Compound and Conc.n (mg/mL) of Fe_2O_3 NPs and Ag-Fe_2O_3NCs		Bacterial strain and zone of inhibition			
		S. aureus ATCC25923	*S. Pyogenes* ATCC19615	*E. coli* ATCC25922	*P. aeruginosa* ATCC27853
Fe_2O_3	100	6	6	9.3	7.6
	50	6	6	7.3	6.6
	25	6	6	6	6
	12.5	6	6	6	6
15SIC	100	18.33	22	21.6	22.6
	50	17.67	17.67	21.6	20.3
	25	16.6	18.3	19	18.6
	12.5	9.3	10.6	10.3	11.66
0.5SIC	100	9.6	10.5	11.6	9.66
	50	9	9	9.3	9.33
	25	8.3	8.66	7.66	8.3
	12.5	7.66	7	7.3	6

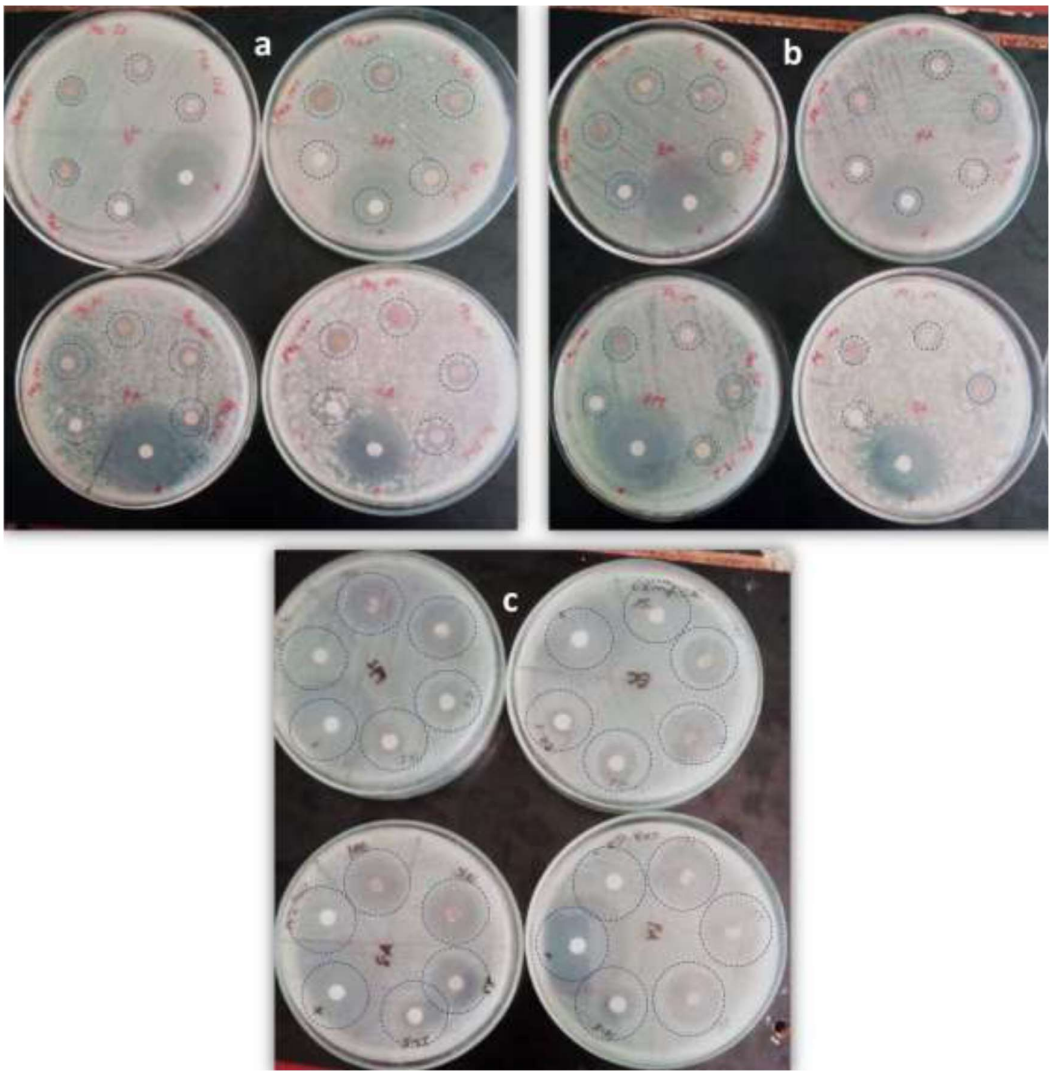

Figure 12. Disk diffusion antibacterial activity evaluation of the sol-gel/combustion synthesized Fe_2O_3(a), 0.5SIC(b) and 15SIC(c) against P. aeruginosa, S. pyogenes, E. coli, and S. aureus.

4.4 Mechanism of Antibacterial Activity

The antimicrobial activity mechanism of NPs may follow three mechanisms including the release of antimicrobial ions (Espitia *et al*., 2012; Kasemets *et al*., 2009), the interaction of NPs with microorganisms (L. Zhang *et al*., 2008), and the formation of ROS by the effect of light radiation (Jalal *et al.,* 2010). The direct contact of NPs with the bacterial cell and production of ROS close to the bacterial membrane that causes damage to bacterial cells has also been suggested to be the other mechanism (Abebe *et al*., 2020; L. Zhang *et al*., 2008). The global

negative charge of the bacterial cells at biological pH was occurred due to the dissociation of carboxylic groups (Stoimenov *et al*., 2002) and metal/metal oxides has positively charged properties (L. Zhang *et al*., 2008). The interaction/electrostatic force that occurred between negatively charged bacterial cells and positively charged metal/metal oxides lead to disruption of the cell wall and damage occurred by entering into the cell. Thakur et al. (Thakur et al., 2019) proposed the direct and indirect mechanism for the interaction of cerium oxide NPs with the bacteria cell. The direct interaction of cerium oxide NPs led to damage to the cell wall and generates ROS inside. Whereas, the indirect mechanism shows the interaction of cerium oxide NPs with the bacterial environment outside the cell and generates ROS that further enters into the cell by damaging the cell wall. Both mechanisms finally led to cell death by affecting the DNA, ribosomes, and proteins of the bacteria. According to this study, since there was no light used as a radiation source, the probable mechanism for bacterial deactivation is due to the release of ions or/and interaction of bacterial cells with NPs or NCs.

5. CONCLUSION AND RECOMMENDATION

5.1 CONCLUSION

In this work, silver iron oxide nanocomposites were successfully sol-gel/combustion synthesized method using silver nitrate ($AgNO_3$) and ferric nitrate ($FeNO_3$)$3.9H_2O$ as a precursor in the presence of stabilized polymer (PVA) within different percent 0.5,1,5,10, and 15. The synthesized SIC and Fe_2O_3 were then characterized by TGA, XRD, UV-Vis, SEM-EDX, PL and FT-IR Spectroscopy. More crystalline nature and best performing SIC were obtained when it was sol-gel/combustion within a 15SIC. Crystalline analysis showed the average crystalline size as 38.76, 41.63, 39.88,37.46 and 34.44nm for 0.5, 1, 5, 10 and 15SIC respectively. The XRD result confirmed the face-centered cubic crystal structure of SICs. All characterization techniques based on XRD results that have small crystalline size. 15SIC show maximum absorption wavelengths were recorded at 590 nm. The energy bandgap values (direct and indirect) for 15SIC was found to be 2.130 and 2.105 eV, respectively. The surface bonding features were confirmed by FT-IR analysis. The antibacterial studies of Fe_2O_3 and 0.5SIC and 15SIC conducted against the gram-negative species, *E. coli*, and *P. aeruginosa*, and gram-positive species, *S. pyogenes*, and *S. aureus* revealed more efficiency for 15SIC. This is due to its small average crystalline size, uniform spherical shape, and large surface region, which creates electronic effects, and these effects can increase the binding strength of the nanoparticles with the bacteria cell membrane. The bactericidal effect of NPs was found to be the same yet slightly higher for Gram-negative bacteria compared to the Gram-positive bacteria. It is due to the difference in the structural composition of Gram-positive and Gram-negative bacteria.

5.2. RECOMMENDATIONS

The following is recommended for the extension of this work:

1. 1.Surface area determination of synthesized nanocomposite for further application in waste water treatment.
2. Toxicity testing of synthesized nanocomposite should be carried out.
3. Leaching test of nanocomposite should also be carried out to use in other application like anticancer activities.

6. REFERENCE

Abbas, M., Naeem, N., Iftikhar, H., & Latif, U. (2018). Synthesis, Characterization and Antimicrobial Properties of Silver Nanocomposites. In *Silver Nanoparticles - Fabrication, Characterization and Applications*. InTech. https://doi.org/10.5772/intechopen.74623

Abd-Elrahman, M. I. (2013). Synthesis of Polyvinyl Alcohol–Zinc Oxide Composite by Mechanical Milling: Thermal and Infrared Studies. *Nanoscale and Microscale Thermophysical Engineering*, *17*(3), 194–203. https://doi.org/10.1080/15567265.2013.776152

Abdulsahib, S. S. (2021). Synthesis, characterization and biomedical applications of silver nanoparticles. *Biomedicine*, *41*(2), 458–464. https://doi.org/10.51248/.v41i2.1058

Abebe, B., & Murthy, H. C. A. (2022). Insights into ZnO-based doped porous nanocrystal frameworks. *RSC Advances*, *12*(10), 5816–5833. https://doi.org/10.1039/D1RA09152B

Abebe, B., Tsegaye, D., & Ananda Murthy, H. C. (2022). Insight into nanocrystal synthesis: from precursor decomposition to combustion. *RSC Advances*, *12*(37), 24374–24389. https://doi.org/10.1039/D2RA05222A

Abebe, B., Zereffa, E. A., & Murthy, H. C. A. (2021). Synthesis of Poly(vinyl alcohol)-Aided ZnO/Mn2O3Nanocomposites for Acid Orange-8 Dye Degradation: Mechanism and Antibacterial Activity. *ACS Omega*, *6*(1), 954–964. https://doi.org/10.1021/acsomega.0c05597

Abebe, B., Zereffa, E. A., Tadesse, A., & Murthy, H. C. A. (2020). A Review on Enhancing the Antibacterial Activity of ZnO: Mechanisms and Microscopic Investigation. *Nanoscale Research Letters*, *15*(1), 190. https://doi.org/10.1186/s11671-020-03418-6

AL-Awadi, S. S., Shbeeb, R. T., & Chiad, B. T. (2018). Effect of Silver Nanoparticles on Fluorescence Spectra of C480 dye. *IRAQI JOURNAL OF SCIENCE*, *59*(1C), 502–509. https://doi.org/10.24996/ijs.2018.59.1C.7

Al-Hakkani, M. F., Gouda, G. A., & Hassan, S. H. A. (2021). A review of green methods for phyto-fabrication of hematite (α-Fe2O3) nanoparticles and their characterization, properties, and applications. *Heliyon*, *7*(1), e05806. https://doi.org/10.1016/j.heliyon.2020.e05806

Al-Zahrani, F. A. M., Salem, S. S., Al-Ghamdi, H. A., Nhari, L. M., Lin, L., & El-Shishtawy, R. M. (2022). Green Synthesis and Antibacterial Activity of Ag/Fe2O3 Nanocomposite

Using Buddleja lindleyana Extract. *Bioengineering*, *9*(9), 452. https://doi.org/10.3390/bioengineering9090452

Alemayehu, T. (2021). Prevalence of multidrug-resistant bacteria in Ethiopia: a systematic review and meta-analysis. *Journal of Global Antimicrobial Resistance*, *26*, 133–139. https://doi.org/10.1016/j.jgar.2021.05.017

Ali, A., Shah, T., Ullah, R., Zhou, P., Guo, M., Ovais, M., Tan, Z., & Rui, Y. (2021). Review on Recent Progress in Magnetic Nanoparticles: Synthesis, Characterization, and Diverse Applications. *Frontiers in Chemistry*, *9*(July), 1–25. https://doi.org/10.3389/fchem.2021.629054

Annu, Ali, A., & Ahmed, S. (2018). Green Synthesis of Metal, Metal Oxide Nanoparticles, and Their Various Applications. In *Handbook of Ecomaterials* (pp. 1–45). Springer International Publishing. https://doi.org/10.1007/978-3-319-48281-1_115-1

Ansari, S. A., Khan, M. M., Ansari, M. O., Lee, J., & Cho, M. H. (2013). Biogenic Synthesis, Photocatalytic, and Photoelectrochemical Performance of Ag–ZnO Nanocomposite. *The Journal of Physical Chemistry C*, *117*(51), 27023–27030. https://doi.org/10.1021/jp410063p

Anzlovar, A. (2015). *Polyol mediated nano size zinc oxide and nanocomposites with poly (methyl methacrylate)*. *May 2011*. https://doi.org/10.3144/expresspolymlett.2011.59

Bayda, S., Adeel, M., Tuccinardi, T., Cordani, M., & Rizzolio, F. (2019). The History of Nanoscience and Nanotechnology: From Chemical–Physical Applications to Nanomedicine. *Molecules*, *25*(1), 112. https://doi.org/10.3390/molecules25010112

Buonsanti, R., Grillo, V., Carlino, E., Giannini, C., Kipp, T., Cingolani, R., & Cozzoli, P. D. (2008). Nonhydrolytic Synthesis of High-Quality Anisotropically Shaped Brookite TiO 2 Nanocrystals. *Journal of the American Chemical Society*, *130*(33), 11223–11233. https://doi.org/10.1021/ja803559b

Buonsanti, R., & Milliron, D. J. (2013). Chemistry of Doped Colloidal Nanocrystals. *Chemistry of Materials*, *25*(8), 1305–1317. https://doi.org/10.1021/cm304104m

Cao, X., & Wang, N. (2011). A novel non-enzymatic glucose sensor modified with Fe2O3 nanowire arrays. *The Analyst*, *136*(20), 4241. https://doi.org/10.1039/c1an15367f

Carlos, E., Martins, R., Fortunato, E., & Branquinho, R. (2020). Solution Combustion Synthesis: Towards a Sustainable Approach for Metal Oxides. *Chemistry – A European Journal*, *26*(42), 9099–9125. https://doi.org/10.1002/chem.202000678

De Matteis, V., Cascione, M., Toma, C., & Leporatti, S. (2018). Silver Nanoparticles: Synthetic Routes, In Vitro Toxicity and Theranostic Applications for Cancer Disease.

Nanomaterials, *8*(5), 319. https://doi.org/10.3390/nano8050319

Demarchi, C. A., Bella Cruz, A., Ślawska-Waniewska, A., Nedelko, N., Dłużewski, P., Kaleta, A., Trzciński, J., Magro, J. D., Scapinello, J., & Rodrigues, C. A. (2018). Synthesis of Ag@Fe2O3 nanocomposite based on O-carboxymethylchitosan with antimicrobial activity. *International Journal of Biological Macromolecules*, *107*(PartA), 42–51. https://doi.org/10.1016/j.ijbiomac.2017.08.147

Domènech, B., Muñoz, M., Muraviev, D. N., & Macanás, J. (2013). Polymer-Silver Nanocomposites as Antibacterial materials. *Microbial Pathogens and Strategies for Combating Them: Science, Technology and Education*, *1*(December), 630–640. papers2://publication/uuid/23AC48BD-C33E-4C2E-8268-3C5E5BF45F57

Espitia, P. J. P., Soares, N. de F. F., Coimbra, J. S. dos R., de Andrade, N. J., Cruz, R. S., & Medeiros, E. A. A. (2012). Zinc Oxide Nanoparticles: Synthesis, Antimicrobial Activity and Food Packaging Applications. *Food and Bioprocess Technology*, *5*(5), 1447–1464. https://doi.org/10.1007/s11947-012-0797-6

Factori, I. M., Amaral, J. M., Camani, P. H., Rosa, D. S., Lima, B. A., Brocchi, M., da Silva, E. R., & Souza, J. S. (2021). ZnO Nanoparticle/Poly(vinyl alcohol) Nanocomposites via Microwave-Assisted Sol–Gel Synthesis for Structural Materials, UV Shielding, and Antimicrobial Activity. *ACS Applied Nano Materials*, *4*(7), 7371–7383. https://doi.org/10.1021/acsanm.1c01334

Fan, X., Yahia, L., & Sacher, E. (2021). Antimicrobial Properties of the Ag, Cu Nanoparticle System. *Biology*, *10*(2), 137. https://doi.org/10.3390/biology10020137

Gao, Y., Meng, F., Li, X., Wen, J. Z., & Li, Z. (2016). Factors controlling nanosized Ni–Al 2 O 3 catalysts synthesized by solution combustion for slurry-phase CO methanation: the ratio of reducing valences to oxidizing valences in redox systems. *Catalysis Science & Technology*, *6*(21), 7800–7811. https://doi.org/10.1039/C6CY01603K

George, J. M., Antony, A., & Mathew, B. (2018). Metal oxide nanoparticles in electrochemical sensing. *Microchimica Acta*, *185*(358), 1–26.

Ghafari, E., Feng, Y., Liu, Y., Ferguson, I., & Lu, N. (2017). Investigating process-structure relations of ZnO nanofiber via electrospinning method. *Composites Part B: Engineering*, *116*(December), 40–45. https://doi.org/10.1016/j.compositesb.2017.02.026

Ghaffari-Moghaddam, M., & Eslahi, H. (2014). Synthesis, characterization and antibacterial properties of a novel nanocomposite based on polyaniline/polyvinyl alcohol/Ag. *Arabian Journal of Chemistry*, *7*(5), 846–855. https://doi.org/10.1016/j.arabjc.2013.11.011

Gordon, T., Perlstein, B., Houbara, O., Felner, I., Banin, E., & Margel, S. (2011). Colloids and

Surfaces A : Physicochemical and Engineering Aspects Synthesis and characterization of zinc / iron oxide composite nanoparticles and their antibacterial properties. *Colloids and Surfaces A: Physicochemical and Engineering Aspects*, *374*(1–3), 1–8. https://doi.org/10.1016/j.colsurfa.2010.10.015

Hasan, M., Banerjee, A. N., & Lee, M. (2015). Enhanced thermo-optical performance and high BET surface area of graphene@PVC nanocomposite fibers prepared by simple facile deposition technique: N 2 adsorption study. *Journal of Industrial and Engineering Chemistry*, *21*, 828–834. https://doi.org/10.1016/j.jiec.2014.04.019

Haseena, S., Shanavas, S., Duraimurugan, J., Ahamad, T., Alshehri, S. M., Acevedo, R., & Jayamani, N. (2020). Study on photocatalytic and antibacterial properties of phase pure Fe2O3 nanostructures synthesized using Caralluma Fimbriata and Achyranthes Aspera leaves. *Optik*, *203*, 164047. https://doi.org/10.1016/j.ijleo.2019.164047

Hong, R. Y., Li, J. H., Chen, L. L., Liu, D. Q., Li, H. Z., Zheng, Y., & Ding, J. (2009). Synthesis, surface modification and photocatalytic property of ZnO nanoparticles. *Powder Technology*, *189*(3), 426–432. https://doi.org/10.1016/j.powtec.2008.07.004

Hoque, M. A., Ahmed, M. R., Rahman, G. T., Rahman, M. T., Islam, M. A., Khan, M. A., & Hossain, M. K. (2018). Fabrication and comparative study of magnetic Fe and α-Fe2O3 nanoparticles dispersed hybrid polymer (PVA + Chitosan) novel nanocomposite film. *Results in Physics*, *10*(June), 434–443. https://doi.org/10.1016/j.rinp.2018.06.010

Hujjatul Islam, M., Paul, M. T. Y., Burheim, O. S., & Pollet, B. G. (2019). Recent developments in the sonoelectrochemical synthesis of nanomaterials. *Ultrasonics Sonochemistry*, *59*(April), 104711. https://doi.org/10.1016/j.ultsonch.2019.104711

Jalal, R., Goharshadi, E. K., Abareshi, M., Moosavi, M., Yousefi, A., & Nancarrow, P. (2010). ZnO nanofluids: Green synthesis, characterization, and antibacterial activity. *Materials Chemistry and Physics*, *121*(1–2), 198–201. https://doi.org/10.1016/j.matchemphys.2010.01.020

Jassby, D., Farner Budarz, J., & Wiesner, M. (2012). Impact of Aggregate Size and Structure on the Photocatalytic Properties of TiO 2 and ZnO Nanoparticles. *Environmental Science & Technology*, *46*(13), 6934–6941. https://doi.org/10.1021/es202009h

Jiamprasertboon, A., Kafizas, A., Sachs, M., Ling, M., Alotaibi, A. M., Lu, Y., Siritanon, T., Parkin, I. P., & Carmalt, C. J. (2019). Heterojunction α-Fe 2 O 3 /ZnO Films with Enhanced Photocatalytic Properties Grown by Aerosol-Assisted Chemical Vapour Deposition. *Chemistry – A European Journal*, *25*(48), 11337–11345. https://doi.org/10.1002/chem.201902175

Jun, Y., Choi, J., & Cheon, J. (2006). Shape Control of Semiconductor and Metal Oxide Nanocrystals through Nonhydrolytic Colloidal Routes. *Angewandte Chemie International Edition*, *45*(21), 3414–3439. https://doi.org/10.1002/anie.200503821

Kasemets, K., Ivask, A., Dubourguier, H.-C., & Kahru, A. (2009). Toxicity of nanoparticles of ZnO, CuO and TiO2 to yeast Saccharomyces cerevisiae. *Toxicology in Vitro*, *23*(6), 1116–1122. https://doi.org/10.1016/j.tiv.2009.05.015

Kayani, Z. N., Arshad, S., Riaz, S., & Naseem, S. (2014). Synthesis of Iron Oxide Nanoparticles by Sol–Gel Technique and Their Characterization. *IEEE Transactions on Magnetics*, *50*(8), 1–4. https://doi.org/10.1109/TMAG.2014.2313763

Khan, A. U., Rahman, A. ur, Yuan, Q., Ahmad, A., Khan, Z. U. H., Mahnashi, M. H., Alyami, B. A., Alqahtani, Y. S., Ullah, S., & Wirman, A. P. (2020). Facile and eco-benign fabrication of Ag/Fe2O3 nanocomposite using Algaia Monozyga leaves extract and its' efficient biocidal and photocatalytic applications. *Photodiagnosis and Photodynamic Therapy*, *32*(August), 101970. https://doi.org/10.1016/j.pdpdt.2020.101970

Khan, H., Habib, M., Khan, A., & Boffito, D. C. (2020). A modified sol-gel synthesis to yield a stable Fe3+/ZnO photocatalyst: Degradation of water pollutants and mechanistic insights under UV and visible light. *Journal of Environmental Chemical Engineering*, *8*(5), 104282. https://doi.org/10.1016/j.jece.2020.104282

Khort, A., Hedberg, J., Mei, N., Romanovski, V., Blomberg, E., & Odnevall, I. (2021). Corrosion and transformation of solution combustion synthesized Co, Ni and CoNi nanoparticles in synthetic freshwater with and without natural organic matter. *Scientific Reports*, *11*(1), 7860. https://doi.org/10.1038/s41598-021-87250-7

Kolahalam, L. A., Kasi Viswanath, I. V., Diwakar, B. S., Govindh, B., Reddy, V., & Murthy, Y. L. N. (2019a). Review on nanomaterials: Synthesis and applications. *Materials Today: Proceedings*, *18*(xxxx), 2182–2190. https://doi.org/10.1016/j.matpr.2019.07.371

Kolahalam, L. A., Kasi Viswanath, I. V., Diwakar, B. S., Govindh, B., Reddy, V., & Murthy, Y. L. N. (2019b). Synthesis and applicatioReview on nanomaterials: ns. *Materials Today: Proceedings*, *18*, 2182–2190. https://doi.org/10.1016/j.matpr.2019.07.371

Kumar, S., Krishnakumar, B., Sobral, A. J. F. N., & Koh, J. (2019). Bio-based (chitosan / PVA / ZnO) nanocomposites fi lm : Thermally stable and photoluminescence material for removal of organic dye. *Carbohydrate Polymers*, *205*(October 2018), 559–564. https://doi.org/10.1016/j.carbpol.2018.10.108

Lassoued, A., Lassoued, M. S., Dkhil, B., Ammar, S., & Gadri, A. (2018). Synthesis, photoluminescence and Magnetic properties of iron oxide (α-Fe2O3) nanoparticles

through precipitation or hydrothermal methods. *Physica E: Low-Dimensional Systems and Nanostructures*, *101*, 212–219. https://doi.org/10.1016/j.physe.2018.04.009

Lee, S., & Xu, H. (2016). Size-Dependent Phase Map and Phase Transformation Kinetics for Nanometric Iron(III) Oxides (γ → ε → α Pathway). *The Journal of Physical Chemistry C*, *120*(24), 13316–13322. https://doi.org/10.1021/acs.jpcc.6b05287

Liu, Y., Zhang, Q., Xu, M., Yuan, H., Chen, Y., Zhang, J. J., Luo, K., Zhang, J. J., & You, B. (2019). Novel and efficient synthesis of Ag-ZnO nanoparticles for the sunlight-induced photocatalytic degradation. *Applied Surface Science*, *476*(September 2018), 632–640. https://doi.org/10.1016/j.apsusc.2019.01.137

Luengo, Y., Sot, B., & Salas, G. (2020). Combining Ag and γ-Fe2O3 properties to produce effective antibacterial nanocomposites. *Colloids and Surfaces B: Biointerfaces*, *194*(June), 111178. https://doi.org/10.1016/j.colsurfb.2020.111178

Madkour, M., Bumajdad, A., & Al-sagheer, F. (2019). To what extent do polymeric stabilizers affect nanoparticles characteristics? *Advances in Colloid and Interface Science*, *270*, 38–53. https://doi.org/10.1016/j.cis.2019.05.004

Mallakpour, S., Abdolmaleki, A., & Moosavi, S. E. (2015). Green Route for the Synthesis of Alanine-based Poly(amide-imide) Nanocomposites Reinforced with the Modified ZnO by Poly(vinyl alcohol) as a Biocompatible Coupling Agent. *Polymer-Plastics Technology and Engineering*, *54*(14), 1448–1456. https://doi.org/10.1080/03602559.2014.996907

Mallakpour, S., & Adnany Sadaty, M. (2016). Preparation and characterization of nanocomposites based on poly(vinyl alcohol) and vitamin B1-modified TiO2 and evaluation of the optical, mechanical, and thermal properties. *Colloid and Polymer Science*, *294*(12), 2099–2107. https://doi.org/10.1007/s00396-016-3974-8

Mathevula, L. E., Noto, L. L., Mothudi, B. M., Chithambo, M., & Dhlamini, M. S. (2017). Structural and optical properties of sol-gel derived α-Fe2O3 nanoparticles. *Journal of Luminescence*, *192*, 879–887. https://doi.org/10.1016/j.jlumin.2017.07.055

Mirzaei, A., Janghorban, K., Hashemi, B., Bonyani, M., Leonardi, S. G., & Neri, G. (2016). A novel gas sensor based on Ag/Fe2O3 core-shell nanocomposites. *Ceramics International*, *42*(16), 18974–18982. https://doi.org/10.1016/j.ceramint.2016.09.052

Mishra, D., Arora, R., Lahiri, S., Amritphale, S. S., & Chandra, N. (2014). Synthesis and characterization of iron oxide nanoparticles by solvothermal method. *Protection of Metals and Physical Chemistry of Surfaces*, *50*(5), 628–631. https://doi.org/10.1134/S2070205114050128

Modwi, A., Taha, K. K., Khezami, L., Boudina, M., Khairy, M., Al-Duaij, O. K., & Talab, S.

(2021). Dependence of the electrical properties of Cu-doped ZnO nanoparticles decorated by Ag atoms. *Zeitschrift Für Physikalische Chemie*, *235*(6), 745–767. https://doi.org/10.1515/zpch-2019-1473

Mulvaney, P. (2015). Nanoscience vs. Nanotechnology. *ACS Nano*, *9*(3), 2215–2217.

Muneer, I., & Farrukh, M. A. (2022). Structural, optical, photoluminescence, photocatalytic and antifungal features of Gd/Mn2SnO4 nanocomposite annealed at different temperatures. *Journal of Materials Science: Materials in Electronics*, *33*(3), 1263–1279. https://doi.org/10.1007/s10854-021-07420-1

Naz, S., Islam, M., Tabassum, S., Fernandes, N. F., Carcache de Blanco, E. J., & Zia, M. (2019). Green synthesis of hematite (α-Fe2O3) nanoparticles using Rhus punjabensis extract and their biomedical prospect in pathogenic diseases and cancer. *Journal of Molecular Structure*, *1185*, 1–7. https://doi.org/10.1016/j.molstruc.2019.02.088

Negrescu, A. M., Killian, M. S., Raghu, S. N. V., Schmuki, P., Mazare, A., & Cimpean, A. (2022). Metal Oxide Nanoparticles: Review of Synthesis, Characterization and Biological Effects. *Journal of Functional Biomaterials*, *13*(4), 274. https://doi.org/10.3390/jfb13040274

Nersisyan, H. H., Lee, J. H., Ding, J.-R., Kim, K.-S., Manukyan, K. V., & Mukasyan, A. S. (2017). Combustion synthesis of zero-, one-, two- and three-dimensional nanostructures: Current trends and future perspectives. *Progress in Energy and Combustion Science*, *63*, 79–118. https://doi.org/10.1016/j.pecs.2017.07.002

Nguyen, N. T. T., An, T. N. M., Pham, S. Q. T., & Cao, X. T. (2022). Synthesis of silver nanoparticles stabilized polymer/graphene oxide for catalytic and antibacterial application. *Molecular Crystals and Liquid Crystals*, *742*(1), 56–63. https://doi.org/10.1080/15421406.2022.2046913

Oldenburg, S. J. (2019). Silver Nanomaterials : Properties & Applications. *Sigma-Aldrich*, 2–5. https://www.sigmaaldrich.com/technical-documents/articles/technology-spotlights/silver-nanomaterials.html

Pallela, P. N. V. K., Ummey, S., Ruddaraju, L. K., Gadi, S., Cherukuri, C. S., Barla, S., & Pammi, S. V. N. (2019). Antibacterial efficacy of green synthesized α-Fe2O3 nanoparticles using Sida cordifolia plant extract. *Heliyon*, *5*(11), e02765. https://doi.org/10.1016/j.heliyon.2019.e02765

Ponnaiah, S. K., Periakaruppan, P., & Vellaichamy, B. (2018). New Electrochemical Sensor Based on a Silver-Doped Iron Oxide Nanocomposite Coupled with Polyaniline and Its Sensing Application for Picomolar-Level Detection of Uric Acid in Human Blood and

Urine Samples. *The Journal of Physical Chemistry B*, *122*(12), 3037–3046. https://doi.org/10.1021/acs.jpcb.7b11504

Prabhu, S., & Poulose, E. K. (2012). Silver nanoparticles: mechanism of antimicrobial. *Int. Nano Lett.*, *2*, 32–41.

Prucek, R., Tuček, J., Kilianová, M., Panáček, A., Kvítek, L., Filip, J., Kolář, M., Tománková, K., & Zbořil, R. (2011). The targeted antibacterial and antifungal properties of magnetic nanocomposite of iron oxide and silver nanoparticles. *Biomaterials*, *32*(21), 4704–4713. https://doi.org/10.1016/j.biomaterials.2011.03.039

Radhamani, A. V., Shareef, K. M., & Rao, M. S. R. (2016). ZnO@MnO 2 Core–Shell Nanofiber Cathodes for High Performance Asymmetric Supercapacitors. *ACS Applied Materials & Interfaces*, *8*(44), 30531–30542. https://doi.org/10.1021/acsami.6b08082

Rahman, M. M., Balkhoyor, H. B., & Asiri, A. M. (2019). Removal of a melamine contaminant with Ag-doped ZnO nanocomposite materials. *New Journal of Chemistry*, *43*(47), 18848–18859. https://doi.org/10.1039/C9NJ04638K

Rahmanian, R., Mozaffari, S. A., & Abedi, M. (2015). Disposable urea biosensor based on nanoporous ZnO film fabricated from omissible polymeric substrate. *Materials Science and Engineering: C*, *57*, 387–396. https://doi.org/10.1016/j.msec.2015.08.004

Rane, A. V., Kanny, K., Abitha, V. K., & Thomas, S. (2018). Methods for Synthesis of Nanoparticles and Fabrication of Nanocomposites. In *Synthesis of Inorganic Nanomaterials* (pp. 121–139). Elsevier. https://doi.org/10.1016/B978-0-08-101975-7.00005-1

Rautela, A., Rani, J., & Debnath (Das), M. (2019). Green synthesis of silver nanoparticles from Tectona grandis seeds extract: characterization and mechanism of antimicrobial action on different microorganisms. *Journal of Analytical Science and Technology*, *10*(1), 5. https://doi.org/10.1186/s40543-018-0163-z

Russell, A. D. (2003). Similarities and differences in the responses of microorganisms to biocides. *Journal of Antimicrobial Chemotherapy*, *52*(5), 750–763. https://doi.org/10.1093/jac/dkg422

Salem, S. S., Hammad, E. N., Mohamed, A. A., & El-Dougdoug, W. (2022). A Comprehensive Review of Nanomaterials: Types, Synthesis, Characterization, and Applications. *Biointerface Research in Applied Chemistry*, *13*(1), 41. https://doi.org/10.33263/BRIAC131.041

Sangaiya, P., & Jayaprakash, R. (2018). A Review on Iron Oxide Nanoparticles and Their Biomedical Applications. *Journal of Superconductivity and Novel Magnetism*, *31*(11),

3397–3413. https://doi.org/10.1007/s10948-018-4841-2

Selvi, J., Mahalakshmi, S., Parthasarathy, V., Hu, C., Lin, Y., Tung, K., Anbarasan, R., & Annie, A. A. (2019). Optical, thermal, mechanical properties, and non-isothermal degradation kinetic studies on PVA/CuO nanocomposites. *Polymer Composites*, *40*(9), 3737–3748. https://doi.org/10.1002/pc.25235

Shehzad, A., Qureshi, M., Jabeen, S., Ahmad, R., Alabdalall, A. H., Aljafary, M. A., & Al-Suhaimi, E. (2018). Synthesis, characterization and antibacterial activity of silver nanoparticles using Rhazya stricta. *PeerJ*, *6*(12), e6086. https://doi.org/10.7717/peerj.6086

Shukla, P., & Saxena, P. (2021). Polymer Nanocomposites in Sensor Applications: A Review on Present Trends and Future Scope. *Chinese Journal of Polymer Science*, *39*(6), 665–691. https://doi.org/10.1007/s10118-021-2553-8

Sivula, K., Le Formal, F., & Grätzel, M. (2011). Solar Water Splitting: Progress Using Hematite (α-Fe2O3) Photoelectrodes. *ChemSusChem*, *4*(4), 432–449. https://doi.org/10.1002/cssc.201000416

Stoimenov, P. K., Klinger, R. L., Marchin, G. L., & Klabunde, K. J. (2002). Metal Oxide Nanoparticles as Bactericidal Agents. *Langmuir*, *18*(17), 6679–6686. https://doi.org/10.1021/la0202374

Thakur, N., Manna, P., & Das, J. (2019). Synthesis and biomedical applications of nanoceria, a redox active nanoparticle. *Journal of Nanobiotechnology*, *17*(1), 84. https://doi.org/10.1186/s12951-019-0516-9

Ullah, A., Yuan, Q., Ahmad, A., Ul, Z., & Khan, H. (2020). Facile and eco-benign fabrication of Ag / Fe2O3 nanocomposite using Algaia Monozyga leaves extract and its ' efficient biocidal and photocatalytic applications Photodiagnosis and Photodynamic Therapy Facile and eco-benign fabrication of Ag / Fe 2 O 3 nano. *Photodiagnosis and Photodynamic Therapy*, *32*(September), 101970. https://doi.org/10.1016/j.pdpdt.2020.101970

Wang, X., Li, Q., Zhou, C., Cao, Z., & Zhang, R. (2019). ZnO rod/reduced graphene oxide sensitized by α-Fe2O3 nanoparticles for effective visible-light photoreduction of CO2. *Journal of Colloid and Interface Science*, *554*, 335–343. https://doi.org/10.1016/j.jcis.2019.07.014

Wu, Z., & Wu, W. (2015). Shape control of inorganic nanoparticles from solution. *Nanoscale*, *8*, 1237–1259. https://doi.org/10.1039/c5nr07681a

Xu, K., Wu, J., Tan, C. F., Ho, G. W., Wei, A., & Hong, M. (2017). Ag–CuO–ZnO metal–

semiconductor multiconcentric nanotubes for achieving superior and perdurable photodegradation. *Nanoscale*, *9*(32), 11574–11583. https://doi.org/10.1039/C7NR03279J

Xu, M., Chen, Y., Hu, W. Y., Liu, Y. T., Zhang, Q. P., Yuan, H., Wang, X. Y., Zhang, J. X., Luo, K. Y., Li, J., & Xiong, G. (2020). Designed synthesis of microstructure and defect-controlled Cu-doped ZnO–Ag nanoparticles: exploring high-efficiency sunlight-driven photocatalysts. *Journal of Physics D: Applied Physics*, *53*(2), 025106. https://doi.org/10.1088/1361-6463/ab4bfd

Yin, Z., Wang, X., Sun, F., Tong, X., Zhu, C., Lv, Q., Ye, D., Wang, S., Luo, W., & Huang, Y. (2017). Aligned hierarchical Ag/ZnO nano-heterostructure arrays via electrohydrodynamic nanowire template for enhanced gas-sensing properties. *Scientific Reports*, *7*(1), 12206. https://doi.org/10.1038/s41598-017-12553-7

Yıldırım, Ö. A., Unalan, H. E., & Durucan, C. (2013). Highly Efficient Room Temperature Synthesis of Silver-Doped Zinc Oxide (ZnO:Ag) Nanoparticles: Structural, Optical, and Photocatalytic Properties. *Journal of the American Ceramic Society*, *96*(3), 766–773. https://doi.org/10.1111/jace.12218

Yusuf, T. L., Orimolade, B. O., Masekela, D., Mamba, B., & Mabuba, N. (2022). The application of photoelectrocatalysis in the degradation of rhodamine B in aqueous solutions: a review. *RSC Advances*, *12*(40), 26176–26191. https://doi.org/10.1039/D2RA04236C

Zahoor, M., Nazir, N., Iftikhar, M., Naz, S., Zekker, I., Burlakovs, J., Uddin, F., Kamran, A. W., Kallistova, A., Pimenov, N., & Ali Khan, F. (2021). A Review on Silver Nanoparticles: Classification, Various Methods of Synthesis, and Their Potential Roles in Biomedical Applications and Water Treatment. *Water*, *13*(16), 2216. https://doi.org/10.3390/w13162216

Zhang, L., Ding, Y., Povey, M., & York, D. (2008). ZnO nanofluids – A potential antibacterial agent. *Progress in Natural Science*, *18*(8), 939–944. https://doi.org/10.1016/j.pnsc.2008.01.026

Zhang, X.-F., Liu, Z.-G., Shen, W., & Gurunathan, S. (2016). Silver Nanoparticles: Synthesis, Characterization, Properties, Applications, and Therapeutic Approaches. *International Journal of Molecular Sciences*, *17*(9), 1534. https://doi.org/10.3390/ijms17091534

Zhang, Z., Wu, Y., Wang, Z., Zhang, X., Zhao, Y., & Sun, L. (2017). Electrospinning of Ag Nanowires/polyvinyl alcohol hybrid nanofibers for their antibacterial properties. *Materials Science and Engineering: C*, *78*, 706–714. https://doi.org/10.1016/j.msec.2017.04.138

Zhang, Z., Wu, Y., Wang, Z., Zou, X., Zhao, Y., & Sun, L. (2016). Fabrication of silver nanoparticles embedded into polyvinyl alcohol (Ag/PVA) composite nanofibrous films through electrospinning for antibacterial and surface-enhanced Raman scattering (SERS) activities. *Materials Science and Engineering: C*, *69*, 462–469. https://doi.org/10.1016/j.msec.2016.07.015